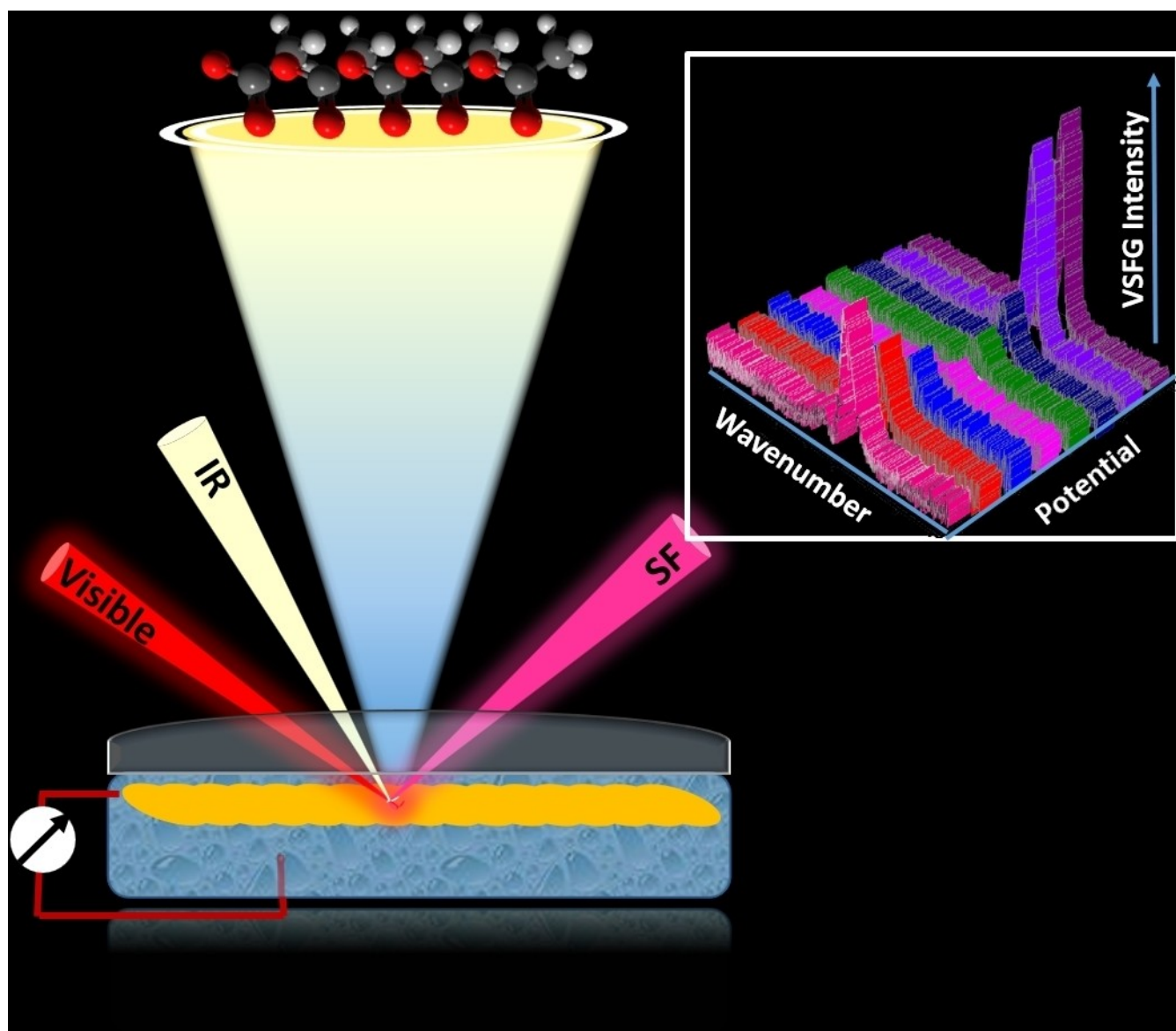


🏆 A Happy Get-Together – Probing Electrochemical Interfaces by Non-Linear Vibrational Spectroscopy

Ratnadip De^[a, b] and Benjamin Dietzek-Ivanšič*^[a, b, c]



Abstract: Electrochemical interfaces are key structures in energy storage and catalysis. Hence, a molecular understanding of the active sites at these interfaces, their solvation, the structure of adsorbates, and the formation of solid-electrolyte interfaces are crucial for an in-depth mechanistic understanding of their function. Vibrational sum-frequency generation (VSFG) spectroscopy has emerged as an operando spectroscopic technique to monitor complex electrochemical interfaces due to its intrinsic interface sensitivity and chemical specificity. Thus, this review discusses the happy get-together

between VSFG spectroscopy and electrochemical interfaces. Methodological approaches for answering core issues associated with the behavior of adsorbates on electrodes, the structure of solvent adlayers, the transient formation of reaction intermediates, and the emergence of solid electrolyte interphase in battery research are assessed to provide a critical inventory of highly promising avenues to bring optical spectroscopy to use in modern material research in energy conversion and storage.

1. Introduction

Electrochemical reactions and technologies are ubiquitous in modern life and society. The rapid growth of electrochemical applications for example in (electro)catalysis,^[1] organic transformation,^[2] environmental protection,^[3] energy storage^[4] and conversion^[5] prompted the development of new electrode materials, modification or functionalization of electrode surface and design of new electrocatalyst.^[6] Unraveling the molecular processes underlying these multiphase electrochemical systems is challenging yet important, as they reveal critical interaction between the electrified surface, adsorbed molecules and the electrolyte layer at the interface.

Electrochemical interfaces, i.e., a key structure in studying any electrochemical reactivity, play a pivotal role in electron and ion transfer. The complex and dynamic nature of electrochemical interfaces^[7] has been studied for a long time – dating back to Helmholtz's formulation of the structure of the electrochemical double layer (EDL), a model that was further advanced by Gouy, Chapman and Stern till the early twentieth century. Classical mean-field descriptions of EDL, as developed by Helmholtz, Gouy, Chapman and Stern account for many experimental observations on a macroscopic scale. However


such models reach their limits, when attempting a realistic representation of each component at the interface, for example charged surface, solvent and ions.^[8] To address this, contemporary studies focus on the chemical and electronic properties of the electrode surface, charge transfer between the electrode and electrolyte while early research was concerned with the distribution of charge/ions across the electrode/electrolyte interface.


Generally, considering electrochemical interfaces for energy conversion and storage, three key levels of structural complexity can be identified: (i) the atomic structure of the electrode surface, (ii) the structure of adsorbed layer, and (iii) the structure of the electrolyte at the interface.^[9] Density, morphology, and composition of the active sites at the interface have proven to be key factors in determining the stability and reactivity of the surface.^[10] However, the structure of adsorbate layers is not solely dependent on the surface morphology or composition, but rather critically depends on the potential applied to the interface. The applied potential modulates the surface charge and the interfacial electric field and, hence, impacts the adsorption^[11] and orientation^[12] of adsorbates as well as the electrolyte layers at the interface which shows manifold effects on electrochemical reactions as observed in several studies.^[13] Since the distance of redox-active species from the electrode surface^[14] and the orientation^[15] of adsorbates can interfere with interfacial electron transfer and structural relaxation processes, a concept of the molecular orientation and reorientation at the electrochemical interface is important to understand the overall reaction kinetics. However, the influence of different aspects is not always separable, rather a complex interplay of adsorbates and substrates was suggested.^[16] For example, studies of the facet-dependent reactivity of the electrode in electrocatalytic CO₂ reduction^[17] or methanol oxidation,^[18] revealed the influence of local electric fields and adsorbate-substrate interactions towards the enhanced activity of certain sites. As observed for electrochemical CO₂ reduction on Au electrode, a higher local electric field generates increased concentration of electrolyte cations near the active sites which led to the stabilization of CO₂ reduction intermediates, thus lowering the thermodynamic barriers of the reaction.^[19] For methanol oxidation, the interaction between electrode adsorbed hydroxide (from water) and CO (from oxidation of methanol) influences the reaction rate.^[18] This interplay of surface and adsorbate structure is highly

[a] R. De, Prof. Dr. B. Dietzek-Ivanšić
Leibniz-Institute of Photonic Technology
Department Functional Interfaces
Albert-Einstein-Straße 9, 07745 Jena (Germany)
E-mail: benjamin.dietzek@uni-jena.de

[b] R. De, Prof. Dr. B. Dietzek-Ivanšić
Institute of Physical Chemistry
Friedrich Schiller University
Helmholtzweg 4, 07743 Jena (Germany)
E-mail: benjamin.dietzek@uni-jena.de

[c] Prof. Dr. B. Dietzek-Ivanšić
Center of Energy and Environmental Chemistry (CEEC Jena)
Friedrich Schiller University
Helmholtzweg 4, 07743 Jena (Germany)
E-mail: benjamin.dietzek@uni-jena.de

 Selected by the Editorial Office for our Showcase of outstanding Review-type articles (www.chemeurj.org/showcase).

 © 2022 The Authors. Chemistry - A European Journal published by Wiley-VCH GmbH. This is an open access article under the terms of the Creative Commons Attribution Non-Commercial NoDerivs License, which permits use and distribution in any medium, provided the original work is properly cited, the use is non-commercial and no modifications or adaptations are made.

dynamic and depends critically, for example, on the investigated potential.^[20] Therefore, experimental tools are required to study electrochemical interfaces at operando conditions with temporal and spatial resolution. However, depending on what kind of process we are interested to observe during an electrochemical reaction the required temporal resolution may be different. For instance- stripping and deposition of ions on a battery electrode can be observed with a resolution of few hundred seconds, while sub-picosecond temporal resolution is needed to observe energy-/charge-transfer between adsorbed molecule and electrode surface.^[21] On the other hand, observing surface morphology and monitoring electro-deposition can be achieved with sub-angstrom to nano meter spatial resolution, which adds to the information obtained in time dependent measurements.^[21b,22]

Our current understanding of electrochemical interfaces builds on a range of experimental methods: Topographical information is obtained by scanning probe techniques such as scanning tunneling microscopy (STM) and atomic force microscopy (AFM). While structural features can be obtained by STM and AFM,^[23] combining these techniques with electrochemical setups, for example scanning electrochemical microscopy (SECM),^[24] electrochemical scanning tunneling microscopy (ECSTM)^[25] adds functional characterization to the nanoscale

and probe local surface conductivity and reactivity of electrode surface.^[24a] X-ray photo electron spectroscopy (XPS),^[26] X-ray absorption spectroscopy (XAS),^[27] and auger electron spectroscopy^[28] yield information about the electronic states of surfaces. Combinations of electron spectroscopy with electrochemistry proved successful in obtaining information on the binding energy of electrolytes/solvents on the electrode surface or the nature of redox-active species at the interface.^[29] Recently, also XPS has been used to identify redox states of electrocatalytically active molecular species on electrodes, for example, for hydrogen evolution,^[26a] CO₂ reduction,^[30] and to characterize battery materials.^[31] However, the electron spectroscopies are somewhat restricted to applications targeting operando conditions, for example, in characterizing solid-electrolyte interfaces. In this respect, optical spectroscopies offer some advantages. For example, surface-enhanced Raman spectroscopy (SERS),^[32] infrared reflection absorption spectroscopy (IRRAS),^[33] and reflection anisotropy spectroscopy^[34] yielded information from the electrode surfaces used in electrochemical oxidation of biomass for example glycerol,^[35] about the Pt/Nafion interface for proton exchange membranes in fuel cells,^[36] Pd-water interface^[37] and also from the solid-electrolyte interphase in Li-ion battery.^[38] Recently, Stimulated Raman scattering has also been emerged as an useful probe for tracking transport of chemical species - like ions near the electrodes in Li-ion battery.^[39]

In situ coupling of optical spectroscopies with electrochemistry has improved our understanding of the dynamic electrochemical interfaces on a molecular level. However, the requirement of roughened substrates for the signal enhancement in SERS limits its applicability in diverse electrode materials.^[40] Also, in linear spectroscopy such as FTIR, overwhelming bulk contribution often obscure the responses inherently originating from the function-determining interface. Thus, interface-specific studies of electrochemical systems under operando condition remains a challenge with linear optical spectroscopic techniques. Hence, by combining the chemical sensitivity of vibrational spectroscopy with the interface-specificity of even order non-linear optical techniques, vibrational sum-frequency generation (VSFG) spectroscopy emerged as a prominent tool to study the electrode-electrolyte interface. The polarization dependency of the VSFG signals stemming from specific vibrational bands of different symmetry enables the determination of molecular orientations at the interface.^[41] Phase-sensitive heterodyne-detected VSFG has proven effective in extracting conformational or orientational information from the molecules at interface.^[42] In addition to its inherent interface specificity, VSFG can probe the temporal evolution of surfaces rendering this technique ideal for in operando studies on electrochemically active surfaces.

This review focuses on the application of VSFG in probing solid-electrolyte interfaces under electrochemical conditions. It addresses a set of key questions, which have been identified in the literature to be elegantly inspected by VSFG. The review will give a brief introduction to VSFG spectroscopy, before describing experimental scenarios to couple VSFG with electrochemistry. We then discuss electrochemical interfaces promoting

Ratnadip obtained his bachelor's in chemistry in 2016 from St. Xavier's College, Kolkata. After that, he joined Indian Institute of Science Education and Research, Kolkata, where he obtained his Master's in Chemical Science and worked as a Junior Research Fellow. Since 2020, he is working as a Ph.D. candidate in the Institute of Physical Chemistry, Friedrich Schiller University, Jena and Leibniz Institute of Photonic Technology, Jena, Germany. His current research is focused on non-linear vibrational spectroscopy at functional interface.



Benjamin Dietzek-Ivanšić studied physics at the University of Wurzburg and the state university of New York at Stony Brook. After his Ph.D. in Physical Chemistry, he joined Lund University and MIT for postdoctoral work. In 2010, he completed his Habilitation in Physical Chemistry at Friedrich Schiller University Jena, Germany. Since 2011 He is a professor for Physical Chemistry -Molecular Photonics and Functional Interfaces at the Friedrich Schiller University Jena. He is the head of the Research Department Functional Interfaces at the Leibniz Institute of Photonic Technology since 2013, where he holds the position of Deputy Scientific Director since 2017. His research is concerned with non-linear spectroscopy and microscopy.



organic transformations, electrocatalysis, and adsorption-desorption processes, where VSFG spectroscopy addresses the structure of adsorbates and interfacial thin layers. Subsequently, mechanistic insights obtained for several key electrochemical reactions, for example, alcohol oxidation, CO₂ reduction are discussed before we highlight the application of VSFG to study electrode-electrolyte interfaces for Li-ion batteries.

2. Background on Vibrational Sum-frequency Generation

2.1. The principle of vibrational sum-frequency generation

Vibrational sum-frequency generation (VSFG) is a non-linear, second-order optical process, where two photons interact with the sample to generate a new photon with a frequency being the sum of the two incident frequencies. The theoretical details of the VSFG process are covered in several reviews^[43] and books,^[44] here we will only give a brief description to introduce the concept to the readers.

Within the dipole approximation VSFG stems from the second-order non-linear susceptibility, it is generated only in systems lacking inversion symmetry. Consequently, it is particularly suited to study surfaces and interfaces, at which intrinsically inversion symmetry is broken. In describing the VSFG signal generation, both the vibrationally resonant ($\chi_{Res}^{(2)}$) and non-resonant susceptibility ($\chi_{NR}^{(2)}$) have to be taken into account (Eq. 1).

$$\chi^{(2)} = \chi_{Res}^{(2)} + \chi_{NR}^{(2)} \quad (1)$$

Among the two incident pulses, if the mid-IR pulse energy matches with a vibrational transition of an IR active vibration of the sample (Figure 1a,b), then the VSFG signal is resonantly enhanced and can be dominated by $\chi_{Res}^{(2)}$. The resonant signal contributions, however, interfere with the non-resonant background, yielding deviations from Lorentzian line shapes. The intensity, $I(\omega)$, of the sum frequency can be expressed as follows:

$$I(\omega) \sim |P^{(2)}(\omega)|^2 \sim |\chi^{(2)}|^2 = |\chi_{NR}^{(2)} + \chi_{Res}^{(2)}|^2 \\ = |A_{NR} \times e^{i\theta} + \sum_n \frac{A_n}{\omega_n - \omega_{IR} - i\Gamma_n}|^2 \quad (2)$$

In Equation (2), A_{NR} and θ are the amplitude and relative phase of the non-resonant susceptibility. A_n is the amplitude of n^{th} vibrational mode and Γ_n represents the line width of the respective vibrational transition. $\hbar\omega_n$ and $\hbar\omega_{IR}$ are the energy of n^{th} vibrational mode and the mid-IR pulse, respectively. From Equation (2), it is evident that the relative phase between the non-resonant and resonant response influences the shape of the VSFG signal.

This interference can be removed in heterodyne-detected VSFG (HD-VSFG), which provides the phase in addition to the

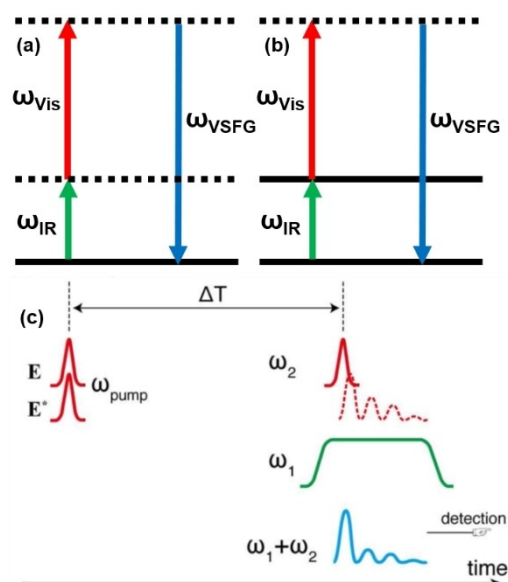


Figure 1. Energy and pulse diagram of (a) non-resonant and (b) resonant VSFG. Dotted and solid lines represent virtual and real energy states respectively (c) Pulse sequence for conventional time-resolved VSFG. (Adapted with permission from Ref. [90], Copyright 2017 American Chemical Society.)

amplitude of the signal and offers more accurate background-free vibrational information as well as information on the molecular orientation at the interface investigated.^[45] Based on the spectral response of VSFG the presence/absence of molecular species at interfaces can be inferred. Additionally, polarization-resolved experiments yield information about molecular orientation. Four different polarization combinations are used in VSFG experiments: *ssp*, *sps*, *pss*, and *ppp* referring to the polarization of sum-frequency signal, visible pulse, and mid-IR pulse, respectively. The ratio between the strength of the vibrational resonance under different polarization combinations can be correlated to the orientation of the transition dipole under consideration.^[41,43,46] Finally, time-resolved vibration sum-frequency generation (TR-VSFG) spectroscopy, which utilizes the VSFG pulse sequence as a probe in a pump-probe scheme (Figure 1c), adds to the tool box of optical nonlinear spectroscopy to study surfaces and interfaces.

While implementing VSFG under electrochemical conditions, an additional electric field will have to be considered in the VSFG process. Under an applied potential (φ), a static electric field E_{DC} is generated at the electrode surface which can influence all the molecules in the double layer near the electrode. In this situation, the effective induced polarization can be approximated as

$$P(\omega) = [\chi^{(2)} \times E_{Vis}(\omega_1) \times E_{IR}(\omega_2)] + [\chi^{(3)} \times E_{Vis}(\omega_1) \times E_{IR}(\omega_2) \times E_{DC}] \quad (3)$$

Depending on the magnitude of the E_{DC} , interference of this third-order term can cause significant spectral changes in the VSFG signal. Furthermore, the decay range of the electric field

in an electrolyte solution can be comparably large, i.e., extending beyond the layer of adsorbed molecules at interface. Hence, the second term in Equation (3) can induce VSFG contribution, not stemming from the surface, and causes potential-dependent changes in the VSFG response under electrochemical conditions. A more detailed theoretical description of the electric field effect can be found elsewhere.^[47] Potential dependent effects on VSFG response and influence of interfacial electric field will be discussed further in the following sections.

2.2. VSFG experiments under electrochemical conditions – some experimental considerations

Generation of the sum-frequency signal requires spatial and temporal overlap of the visible and the mid-IR pulse. (Although in many implementations an 800 nm pulse is used, we will refer to this pulse as “visible” throughout the manuscript.) A conventional VSFG spectroscopy setup is based on a picosecond (ps) or femtosecond (fs) pulsed laser system. In ps-scanning VSFG, a narrow band mid-IR pulse with a spectral bandwidth of a few cm^{-1} is scanned over the range of the vibrational resonance of the molecular species of interest. The narrow band mid-IR pulse is overlapped with a spectrally narrow visible pulse to yield the sum-frequency signal. On the other hand, fs-VSFG schemes use a broad band mid-IR pulse with a spectral bandwidth of 150–250 cm^{-1} to overlap with a range of vibrational resonances. The signal is then spectrally dispersed and detected using either a photomultiplier tube or a CCD detector. Heterodyne detection of VSFG signals can be achieved by overlapping a local oscillator (LO) with the VSFG signal. A more detailed description of homodyne and heterodyne detected VSFG setup is well described in the literature.^[21b,45, 48]

Successful implementation of VSFG under electrochemical conditions requires a spectroelectrochemical cell. For both the visible and mid-IR pulse to reach the electrode surface, an IR-transmitting quartz window is used. The base of the cell is usually fabricated of an inert polymer such as Kel-F or polypropylene.^[42a,49] To allow detection of gaseous reaction products under operando conditions, gas inlets and outlets can also be integrated into the cell. Figure 2 depicts such a design. Air/moisture-sensitive electrochemical reactions can be performed in these cells by creating an inert or nitrogen chamber with an additional window for transmitting the beams.^[50] For the incoming laser beams and the resulting VSFG signal, two types of reflection geometry can be implemented, which depend on the nature of the working electrode. Both, application and limitation of these two modes can be found well recorded in the literature.^[51]

For example, for highly reflecting or non-transparent electrodes, an external reflection of the beams is used. In external reflection mode, a thin layer of electrolyte is pressed between the working electrode and the CaF_2 window (Figure 3a). The width of the layer can be controlled by a Teflon spacer.^[49] Maintaining a thin electrolyte layer minimizes attenuation of the mid-IR pulse and hence increases the VSFG signal.

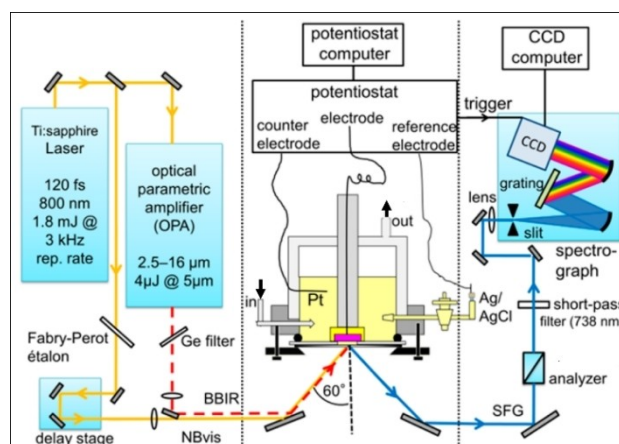


Figure 2. Schematic representation of a spectroelectrochemical VSFG setup realizing the external reflection geometry. Key: BBIR: broad-band mid-infrared pulses. NBvis: narrow-band visible (800 nm) pulses. SFG: Sum-frequency generated signal. (Reproduced with permission from Ref. [87], Copyright 2015 American Chemical Society.)

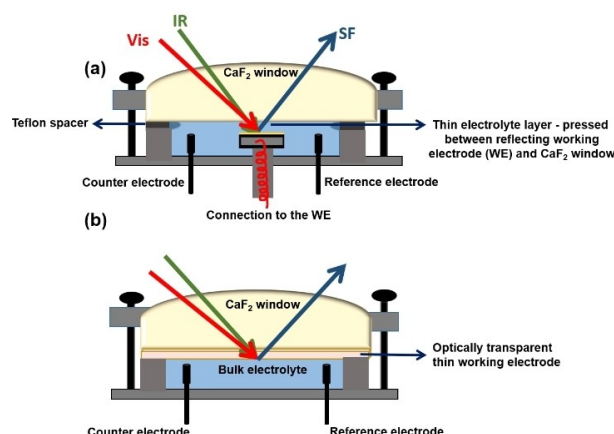


Figure 3. Cross-section of an electrochemical cell (a) an external reflection geometry with highly reflecting electrode (b) internal reflection geometry with optically transparent electrode.

However, the cell design also has to ensure that the electrochemical processes do not get distorted by the ultra-thin solvent/electrolyte layer.^[52] Such complications involved in external reflection experiments can be avoided by using an optically transparent electrode allowing an internal reflection of the beams. Here, the signal originates from the interface between bulk electrolyte and inner surface of the electrode which is coated onto the surface of the CaF_2 window of the cell (as shown in Figure 3b). This method is more practical with transparent battery electrode materials like LiCoO_2 ,^[53] carbon films,^[54] or layered graphene.^[55] Along these lines VSFG was combined with surface plasmon enhancement at the electrode surface.^[56] Liu et al. reported SP enhancement of the VSFG process where the incident angle of the mid-IR pulse on the IR-transparent prism was optimized to excite the SP wave at the electrochemical interface.^[56] Similarly, VSFG experiments were conducted without requiring any thin electrolyte layer by

excitation of a surface plasmon on nano grating engraved metal electrode^[57] and Au thin film.^[58]

3. VSFG at Electrochemical Interfaces

3.1. Electrochemical transformation and catalysis

One of the first applications of VSFG to electrochemical systems was reported by Guyot-Sionnest and Tadjeddine in 1990, who monitored the adsorption of CN^- on a polycrystalline Pt electrode upon varying the electrode potential.^[59] Using a spectroelectrochemical cell with CaF_2 windows and a 1 μm thin layer of the aqueous KCN electrolyte, the adsorption of CN^- on Pt electrode was found to take place in two distinct adsorption modes with either the C or the N bound to the Pt surface, depending on the applied potential (Figure 4a).^[59] Since then the method has advanced significantly towards probing structure and dynamics at a variety of electrochemical interfaces.

Chapter 3.1 will discuss the contributions of VSFG to deciphering the nature of adsorbate molecules on the electrode, focusing on their mode of adsorption and orientation. Subsequently, we describe the structure of the water molecules adjacent to an electrode in a variety of aqueous electrochemical systems and focus on the influence of the electric field on interfacial phenomena. Finally, the last two sections of this chapter are dedicated to the use of steady-state and time-resolved VSFG for mechanistic interpretation of electrochemical reactions.

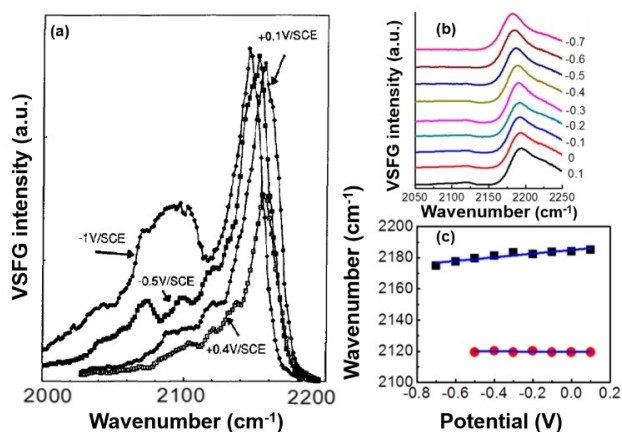


Figure 4. (a) VSFG response from adsorbed CN^- on Pt electrode obtained after cycling between +0.5 V/SCE and -1 V/SCE. (b) Potential dependent VSFG spectrum of 1,4-phenylene diisocyanide, potentials are given vs. Ag/AgCl, (c) potential dependent frequency shift of bound (black square) and free (red circle) NC group of 1,4-phenylene diisocyanide. (Figure 4a is reproduced with permission from Ref. [59], Copyright 1990 Elsevier; Figure 4b–c are Adapted with permission from Ref. [50], Copyright 2017 American Chemical Society)

3.1.1. Molecular structure of adsorbates on electrode surfaces

Adsorption of solvent or electrolyte molecules strongly impacts the performance of any functional electrode surface.^[60] Adsorbates on electrodes, for example, modulate the electronic properties of the surface and regulate its stability, and influence both the thermodynamics and kinetics of the electrochemical reactions. For example, electrode-adsorbed hydrogen critically determines the product selectivity in CO_2 reduction,^[61] while the adsorbed oxygenated species control the kinetics of oxygen reduction.^[62] During electrochemical reactions, the combination of inevitable mass^[63] and charge transport^[64] changes the electrode surface dynamically.^[65] Since VSFG is sensitive to detect less than a monolayer of molecules adsorbed on a surface,^[66] operando VSFG allows following these dynamic changes by the means of chemical composition of the interfacial layer and the orientation of the adsorbates.

Following up on their seminal work mentioned above, Tadjeddine and coworkers, studied the potential-dependent adsorption of CN^- on Ag by VSFG.^[67] In this case, the vibrationally non-resonant (NR) response of the electrode surface showed well-defined minima upon scanning the electrode potential from -1.5 V to 0 V vs. Ag/AgCl. The NR VSFG signal originates either from the intraband or interband electronic transition in the metal substrates.^[68] Near the point of zero charge, the NR response becomes minimal due to the decreased polarizability of the mobile charges in the metal.^[69] Hence, the amplitude of the non-resonant VSFG becomes a direct means of the point of zero charge of the electrode surface in the presence of adsorbates. The vibrational band shifts observed in the resonant VSFG signal reflect the Stark tuning of the vibrational modes and potential-dependent preferential binding of the adsorbates to the surface.

Studying self-assembled monolayers of small organic molecules facilitates the analysis of VSFG signals to disentangle different adsorption modes of adsorbates, for example, the cyanide ($-\text{CN}$) or isocyanide ($-\text{NC}$) moiety on metal electrodes. For example, the VSFG spectrum of the Au/1,4-phenylene diisocyanide/aqueous electrolyte interface showed two distinct peaks at ca. 2180 cm^{-1} and 2128 cm^{-1} originating from metal bound and free NC groups, respectively (Figure 4b, c).^[50] The frequency shift between bound and unbound species depends on the identity of the substrate and binding geometry of the adsorbates.^[70] Another difference stems from the different distances of the vibrational mode of interest relative to the metal surface when comparing bound and unbound groups in VSFG. Due to the larger distance of the free NC from the electrode, changes in the potential of the electrode cause a minor impact of the resulting field on the vibrational mode. As a result, the frequency of the bound NC group was found to be blue-shifted by 16 $\text{cm}^{-1}\text{V}^{-1}$ with the applied potential compared to just 1 $\text{cm}^{-1}\text{V}^{-1}$ shift for the free NC group (Figure 4b).^[50]

Following their work with CN adsorption, Tadjeddine and co-workers monitored dissociative adsorption of methanol on a Pt electrode, resulting in the formation of adsorbed CO .^[67] Adsorption of CO in a linear or bridged geometry (Figure 5a)

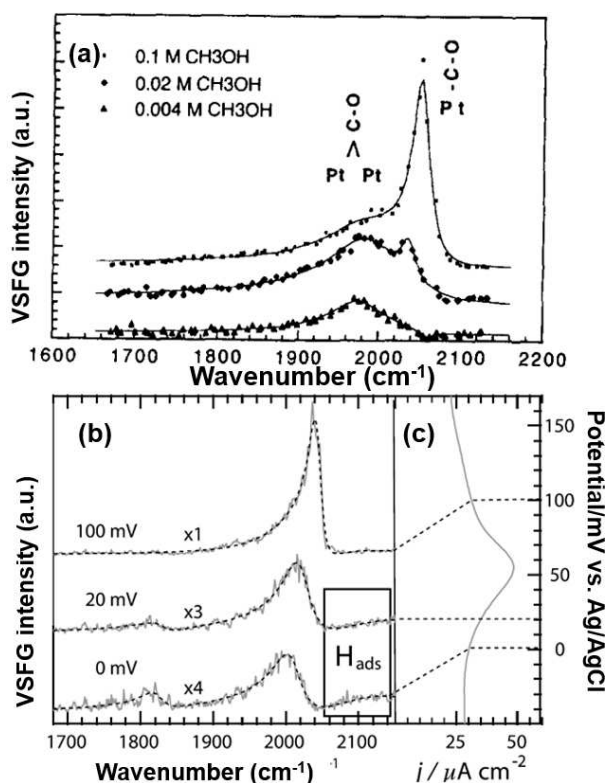


Figure 5. (a) VSFG spectra of CO/Pt in HClO₄ (0.1 M) as a function of the CH₃OH concentration. Spectra were recorded at 0.24 V vs. NHE showing two different adsorption modes. (b) Normalized SFG spectra of the Pt (1 0 0) surface in a solution of 0.01 M methanol in 0.1 M sulfuric acid as a function of the applied potential, a change in the SFG response between 20 mV and 100 mV indicates a different configuration for CO adsorption. (c) Corresponding voltammogram showing that current peak appears at the same region where the configurational change of CO adsorption happens. (Figure 5a is reproduced with permission from Ref. [67], Copyright 1995, Elsevier and Figure 5b–c are reproduced from Ref. [71], Copyright 2004 Elsevier)

yields discernible VSFG spectra.^[67] The relative occupation of each of the binding sites was found to depend on the methanol concentration in the electrolyte, which imparts the possibility of a dynamic equilibrium between the species in solution and adsorbed on the electrode. Influence of electrode adsorbed hydrogen and applied potential on the adsorption of CO resulting from dissociative adsorption^[71] and electrooxidation^[72] of methanol was explored by Vidal et al. in a wide range of potential starting from –150 mV to 900 mV vs. AgCl. At lower potential, adsorbed hydrogen atoms were found to block atop terrace sites on the Pt (1 0 0) surface, thus allowing dissociative adsorption of methanol (into CO) only at step and bridge sites, whereas increasing potential allows hydrogen desorption and subsequent adsorption of methanolic CO in atop sites on terrace (as shown in Figure 5b, intensity of peak at 2040 cm⁻¹ originating from CO adsorbed on atop terrace sites increases with increasing potential, Figure 5c shows corresponding voltammogram).^[71]

Methanol oxidation at a Pt(110) electrode from an electrolyte consisting of 0.1 M methanol in 0.1 M sulfuric was monitored by the potential dependent VSFG signatures of CO

between –150 mV and 900 mV vs. Ag/AgCl.^[72] Thereby, Vidal et al. showed that an increasingly positive potential favors a densely packed and ordered CO layer on the Pt electrode.^[72]

From the above-mentioned CO adsorption studies, a correlation between the positively charged surface and the onset potential of bulk electrooxidation of methanol was observed. A positively charged surface favors the adsorption of oxygen-containing species on the electrode and thus influences the interfacial oxidation reaction. (More work on the role of surface charge will be discussed in the following sections.) Associated with the potential controlled change of surface coverage, also the spectral position and line shape of C–O stretching vibration changes (Figure 6). The frequency shifts indicate the presence of a vibrational Stark effect^[73] and altered dipole-dipole interactions,^[74] the latter one as a consequence of the altered surface coverage. In addition, the potential-dependent charging of the electrode impacts the line shape as indicated above. Depending on the electronic polarizability of the electrode, the contribution of the non-resonant background changes (being minimal at the point of zero charge) and hence, causes changes in the VSFG line shape (Figure 6).

Lu et al. conducted a study on CO oxidation on a Pt electrode using broad-band fs-VSFG. They compared the signatures of the electrochemical interface from electrolytes, which were either saturated with CO or CO-free.^[49] The broad-band VSFG approach eliminates the need for a wavelength scan of the mid-IR pulse and improves the synchronization between potential changes and spectroscopic measurements, for example, during cyclic voltammetry measurements. Following the amplitude of CO vibration in the VSFG signal, Lu et al. could monitor the surface coverage of the adsorbed CO. Taking into account not only the amplitude but also the full width at half maxima, and the Stark tuning of the vibrational signature of the

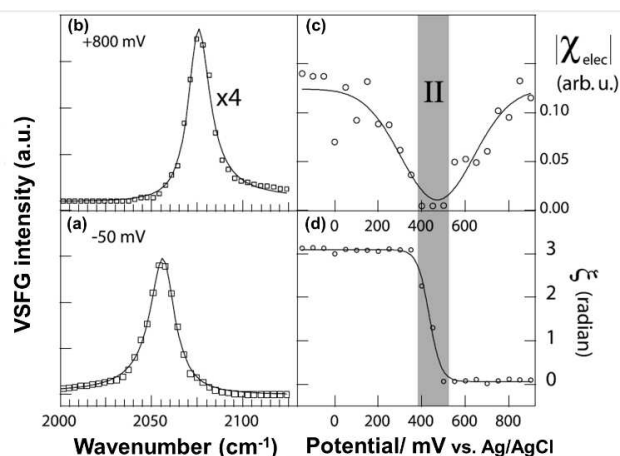


Figure 6. Fitted SFG spectra of CO/Pt at –50 mV (a) and 800 mV (b) (signal multiplied by a factor of 4 for clarity) showing the change in the asymmetry of the peak. Potential dependent (c) amplitude and (d) relative phase of the non-resonant response. Potential dependency of NR background inhibits direct co-relation between surface coverage and SFG peak area/intensity for the potential dependent-VSFG, but from the fitting results, a better analysis of NR and resonance signal is possible. (Reproduced with permission from Ref. [72], Copyright 2005 Elsevier.)

adsorbate, it is possible to deduce the stability of the adsorbed layer against the applied potential. This was realized by Humbert et al. while studying the CO poisoning on Pt electrode surface.^[75] It was noticed that dense packing of CO on the electrode inhibits the adsorption of hydrogen or any oxidative species, thus quenching hydrogen evolution and inhibiting the oxidation of CO.^[75] Potential-dependent VSFG spectra revealed a stability window of the CO adlayer from -1.2 V to $+1.5$ V vs. Ag/AgCl in a CO saturated solution.

VSFG is not only capable of monitoring molecular adsorption on electrodes, it rather also provides information on the orientation and reorientation of the adsorbates in response to external stimuli. Due to the importance of the molecular orientation on any specific surface chemistry,^[76] this parameter has been studied not only by VSFG but also by, for example, surface enhanced^[77] and tip-enhanced Raman spectroscopy (SERS and TERS).^[78] However, application of SERS is mostly limited to the electrochemistry on roughened gold, copper, and silver electrodes while in case of TERS, reproducibility of the tips imposes some major constraints.^[79] Also, applying these techniques in liquid interface still requires substantial instrumental development.^[80] On contrary, VSFG were found suitable to track molecular reorientation dynamics even at buried interfaces, without requiring any specific electrode type.^[81]

The first application of VSFG to study a reversibly switchable surface, utilizing the applied potential as the external trigger, was reported by Lahann et al.^[82] They examined a low-density self-assembled monolayer of 16-mercapto hexadecanoic acid (MHA) on Au substrates; VSFG signals at 2855 and 2925 cm^{-1} indicated a gauche conformation of the methylene groups in the presence of a non-polar medium, while a more symmetric orientation was observed in a polar environment such as water or acetonitrile (Figure 7).^[82] Such rearrangement of the methylene groups could also be induced by applying electrical potential as external stimulus: A positive potential on the Au surface created the gauche conformation even in a polar medium by field-induced intramolecular rearrangement of the adsorbates, i.e. bending the negatively charged portion of the molecules towards the positively charged electrode. The potential-dependent molecular responses at electrode surfaces

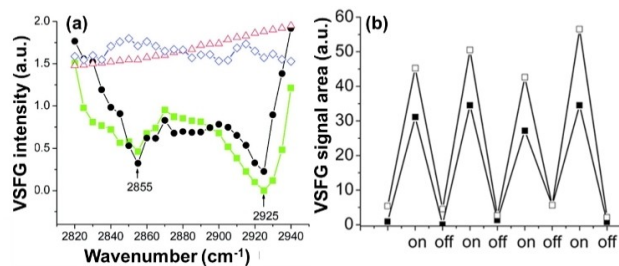


Figure 7. (a) In-situ VSFG spectra of the CH-stretch region (2820 to 2940 cm^{-1}) for the low-density SAM of MHA exposed to air (green squares), d^3 -acetonitrile (red triangles), d^2 -water (blue diamonds), and d^8 -toluene (black circles). (b) Relative VSFG peak area of the methylene modes at wavelengths of 2855 cm^{-1} (solid symbols) and 2925 cm^{-1} (open symbols) for the low-density SAM when a $+25$ mV (vs. SCE) potential was repeatedly applied. (Reproduced with permission from Ref. [82], Copyright 2003 AAAS)

were further studied in electrochemical systems consisting of ionic liquids,^[83] zwitterionic molecule,^[84] and coordinating anions^[85] at metal electrodes. A large set of experiments deals with the structure of ionic liquids at an electrode surface. Exemplarily, Baldelli, and coworkers studied the orientation of the adsorbed cation of an ionic liquid at a Pt electrode upon variation of the electrode potential.^[83] They utilized a room temperature ionic liquids, for example, 1-butyl-3-methylimidazolium [BMIM]⁺ with [PF₆]⁻ or [BF₄]⁻, and examined the C–H stretching peak intensity under different polarization as the electrode potential is varied (Figure 8).^[83]

Comparing the VSFG intensity in *ssp* and *ppp* polarization (Figure 8) the authors concluded that potential changes lead to the reorientation of the organic cations [BMIM]⁺ at the surface. For example, at potentials above pzc, i.e., at positive surface charges, the anions, [PF₆]⁻ or [BF₄]⁻ will move into the inner Helmholtz layer for compensating the charge. To allow this movement the BMIM cation is tipped along the surface normal. Subsequent work showed that such potential-dependent structural transition of ionic liquids is also influenced by the presence of water in the electrolyte.^[52] Studying a related ionic liquid utilizing different anions on a Pt electrode, Zhou et al. focused on the potential dependent adsorption/desorption of the anions, i.e. trifluoromethanesulfonate.^[86] Their observation suggested the presence of a diffuse ion layer in addition to the single ion layer reported earlier.^[86] The potential-dependent VSFG intensity of the 'SO₃' stretching vibrations indicate an adsorption/desorption hysteresis of anions, which originates from the potential energy barrier associated with binding energy and Madelung potential (Madelung constant) of the ions.^[86]

A change in potential can also influence the mode of coordination of the adsorbate: Braunschweig et al.^[85] observed

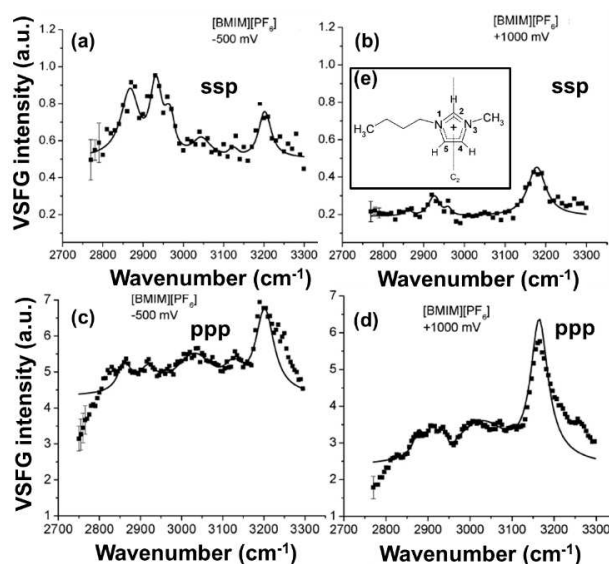


Figure 8. VSFG response of the cation of [BMIM][PF₆] at a Pt electrode recorded at different potentials (vs. Ag/AgPF₆) with *ssp* and *ppp* polarization. (e) Structure of the cation (Reproduced with permission from Ref. [83], Copyright 2004 American Chemical Society)

surface transformations on a Pt electrode at 0.21 V vs. Ag/AgCl resulting from the configurational changes in the (bi)sulfate adlayer. Due to the negligibly low dipole moment perpendicular to the Pt surface, the two-fold coordinated state of the bi(sulfate) was found to be SFG inactive but a potential induced configuration change from the two-fold to a three-fold coordinated state resulted in a strong VSFG signal from the S–O stretching vibration.^[85]

However, the impact of the surface potential on molecular adsorbates is not restricted to charged species. Even molecules with no net charge such as zwitterionic species can reorient themselves upon changes in the surface potential because of their large dipole moment. This was exemplified in a study with p-aminobenzoic acid (PABA) at an Ag(111) electrode. In this system, a potential change across the point of zero charge causes a distinct reorientation of the molecular dipole as reflected in the VSFG signal in the aromatic CH stretch region (Figure 9).^[84] In addition to a flip in the sign of the VSFG signal (upon changing the potential from below to above the point of zero charge), a blue shift of the COO[−] stretching mode is observed at increasingly positive potentials.

However, this was not a gradual frequency shift with potentials as would have originated from the Stark effect, rather a sudden increase in frequency was observed. This was associated with the formation of a densely packed molecular

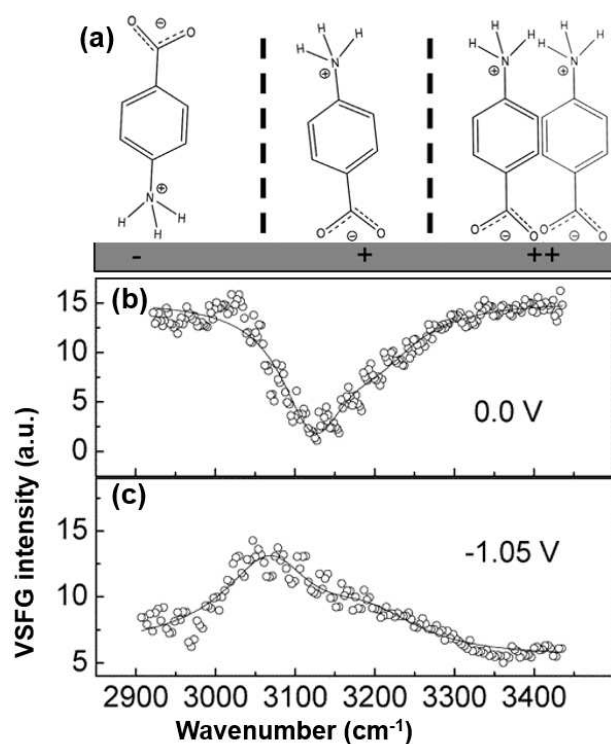


Figure 9. (a) Graphical representation of the potential-induced orientation of p-aminobenzoic acid. (b) SFG spectrum of aromatic CH stretches at Ag(111) in 20 mM PABA and 0.1 M KF at 0.0 V and (c) at −1.05 V (vs. Ag/AgCl). Transformation of spectral feature from a peak to dip at relatively positive potentials suggests flipping of the molecule as it goes through the pzc. (Adapted with permission from Ref. [84], Copyright 2005 American Chemical Society)

layer at higher positive potentials altering the intermolecular interactions. Such structural reorientation at a modified electrode potential can not only influence the structure of the adsorbate layer but also rather impact the course of an electrochemical reaction. This was exemplified by Rey et al. working on CO₂ reduction in an ionic liquid medium at a Ag electrode,^[87] where structural transition of the ionic liquid within the double layer stabilizes CO₂ reduction intermediates and lowers the energy barrier for initial steps.^[88]

To study the absolute orientation of molecules at a surface or interface, heterodyne detected VSFG (HD-VSFG) has been identified as a suitable tool.^[89] HD-VSFG detects the field of the VSFG signal and, hence, allows for treating the imaginary part ($\text{Im } \chi^{(2)}$) of the signal separately from the real part ($\text{Re } \chi^{(2)}$). Thereby, the absolute orientation of molecules can be determined at surfaces and interfaces.^[90] Investigations of, for example, the adsorption geometry of Rhenium-complex-based CO₂ reduction catalyst on TiO₂ semiconductor surfaces^[91] illustrated that the length of the molecular linker determined the spatial orientation of the catalysts relative to the surface. This knowledge can be transferred to developing electrocatalyst-semiconductor systems with a preferred molecular arrangement.^[91]

Sayama et al. utilized HD-VSFG to observe potential-dependent structural changes in an electrode-electrolyte interface^[42a] focusing on co-adsorption studies of acetonitrile (Figure 10) and the CF₃SO₃[−] anion from a LiCF₃SO₃ electrolyte on a Pt electrode. During modulation of the surface charge by applying an external potential, electrolyte anions were found to adsorb only at positive potentials. At those potentials, the CH₃ groups of the acetonitrile molecules were directed towards the anion on the electrode. The authors also highlighted the fact

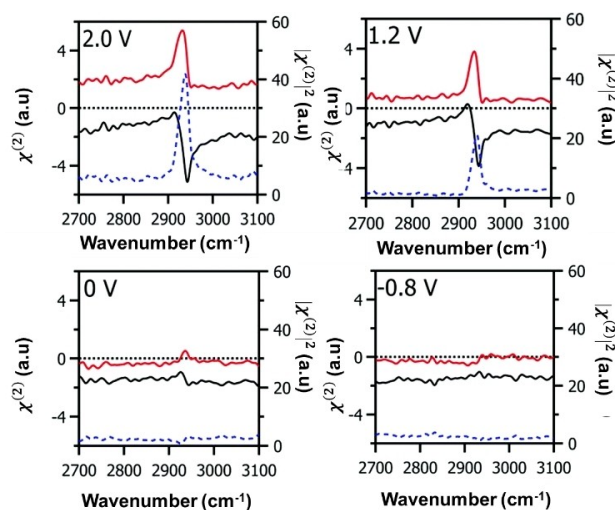


Figure 10. Potential (Ag/Ag⁺) dependent $\text{Im } \chi^{(2)}$, $\text{Re } \chi^{(2)}$ and $|\chi^{(2)}|^2$ spectra of the acetonitrile/platinum interface with a 0.1 M LiCF₃SO₃ electrolyte in the CH stretch region. The red curve, black curve, and blue broken curve are $\text{Im } \chi^{(2)}$, $\text{Re } \chi^{(2)}$, and $|\chi^{(2)}|^2$, respectively. $|\chi^{(2)}|^2$ spectra were calculated from $\text{Im } \chi^{(2)}$ and $\text{Re } \chi^{(2)}$ spectra. At positive potentials the positive CH band in $\text{Im } \chi^{(2)}$ spectrum indicates CH₃ down orientation of acetonitrile, this band disappeared while going towards negative potentials. (Reproduced with permission from Ref. [42a], Copyright 2020 Royal Society of Chemistry)

that without complete knowledge of molecular hyperpolarizability, a combined theoretical study is necessary to complement the experimental observations.

Clark et al. followed such a combined experimental-theoretical approach to determine the molecular orientation of cyano substituted rhenium bipyridine tricarbonyl catalysts, which were weakly bound to an Au electrode.^[92] However, this weakly bound complex dissociated from the surface before any electrochemical process took place as a result of the applied potential. For molecules covalently attached to the electrode, for example thiol substituted Re- and Mn-complexes, the electrode surface can be interrogated in real-time while applying potential without causing the dissociation of the molecules.^[93] Direct attachment of the molecular catalyst to the electrode surface resulted in a pronounced Stark shift of the carbonyl stretching mode while applying a potential to the electrode. By comparing the observed shift in frequency with theoretically calculated Stark tuning rates the value of the interfacial electric field was determined to be ca. 10^8 to 10^9 V m⁻¹. The computed SFG spectra were scanned through a range of tilt (θ) and twist (ψ) angles suggested by the theoretically optimized configurations of the catalyst to obtain the best fit with experimental results. Thus from the comparison of the calculated spectra and experimental VSFG results, the absolute orientation of the molecules attached on the surface was obtained.^[93]

3.1.2. The structure of water at electrode surfaces

Key to a mechanistic understanding of electrochemical processes in aqueous systems is an in-depth knowledge of the structure and dynamics of water itself. In the last decades, different aspects of water structure have been studied both experimentally and theoretically,^[94] for example, in heterogeneous catalysis^[95] and fuel cells.^[96] VSFG has been extended to study the interface between water or aqueous electrolytes and electrified metals. For instance, Tadjeddine and co-workers detected adsorbed hydrogen species on a Pt electrode which was hydrogen-bonded to two water molecules from the adlayer.^[97] However, such experiments are challenging, as detection of a resonant VSFG signal from interfacial water is affected by the absorption of mid-IR pulse by the aqueous solvent itself. In addition to the absorption of the IR intensity by bulk water, the overwhelming non-resonant VSFG response from the metallic electrode complicates the detection of the resonance signal from the electrode interface with water. To address these issues Nihonyanagi et al. implemented VSFG in internal reflection geometry while using both tunable visible and mid-IR light sources.^[98] By modulating the wavelength of the visible light they were able to minimize the non-resonant response of the ultrathin Au electrode, while the internal reflection geometry minimized parasitic IR absorption by bulk water.

Resolving the interference between the resonant and non-resonant VSFG response, information about the polar orientation of water at the interface was obtained. The major resonance peak was centered at 3500 cm⁻¹ and was attributed

to the O–H stretching of liquid-like, less ordered water. A shoulder at 3250 cm⁻¹ originated from tetrahedrally coordinated ice-like, ordered water. A comparison between the VSFG response from these two peaks indicates the extent of ordering in the interfacial H₂O layer.^[99] A potential-dependent VSFG study in the range of -0.2 V to 1.0 V vs. Ag/AgCl showed that the relative phase between the resonant and non-resonant response does not change abruptly in the given potential range. This indicates that the net dipole of the water molecule does not flip in this potential window. Nonetheless, the modulation of the resonant VSFG signal as a function of the applied potential (Figure 11a) indicates structural changes in the interfacial water layer. These structural changes were related to the net charge and the interfacial structure between the electrode and the adlayer.^[98] Such charge-sensitive orientation of the water molecules was also observed on non-conductive surfaces,^[100] which can be related to the lower resonant VSFG response at the point-of-zero charge, as in absence of net surface charge, the water molecules in the adlayer are less organized. Following the work by Nihonyanagi et al.,^[98] Gewirth and co-workers identified a range of water structures at electrified Ag/water interfaces (Figure 11b–d).^[101] In addition to liquid-like water with a low level of hydrogen bonding (characterized by a VSFG peak near 3370 cm⁻¹) adsorbed water molecules were identified yielding a VSFG peak at 2970 cm⁻¹. The shift of the O–H stretching vibration to lower frequencies results from the specific adsorption of the water molecules to the Ag surface and a consequently reduced electron density in the O–H bond. Also, the dependency of this peak on the electric field indicates its association with Ag surface-bound water. Another peak associated with ice-like ordered water was observed at 3250 cm⁻¹, which shows minimal intensity at the point-of-zero charge. This peak was associated with water molecules solvating ionic species, for example Na⁺, F⁻ near the interface, which is less populated near point-of-zero charge. The fourth peak at 2800 cm⁻¹ is observed near the point-of-zero charge and becomes more intense upon increasingly negative potentials. Thus, this peak was ascribed to hydronium species. The potential-dependent VSFG response from the water adlayer, suggests a parallel orientation of water in the absence of any net surface charge. However, the work could not determine the orientation of the molecular dipoles quantitatively, as only a single polarization geometry was investigated and, in the absence of strong non-resonant signal contributions, it was not possible to relate the phase of the resonant signal to the one of the non-resonant contribution.

A comparative study addressing water at Au and Pt electrodes highlights the impact of the metal on the structure of water molecules in the interfacial water layer. The intensity ratio between peaks associated with liquid-like and ice-like water can be taken as a measure to deduce the overall order of water molecules at different metal surfaces.^[102] Microscopic images show well-ordered H₂O films on a clean Pt surface^[103] while amorphous water layers are observed on Au.^[104] At increasingly positive potential, when metal oxides start to be formed, the O–H peak decreases on both electrodes, however, when studying the Au electrode a sharp peak appears at 3550 cm⁻¹

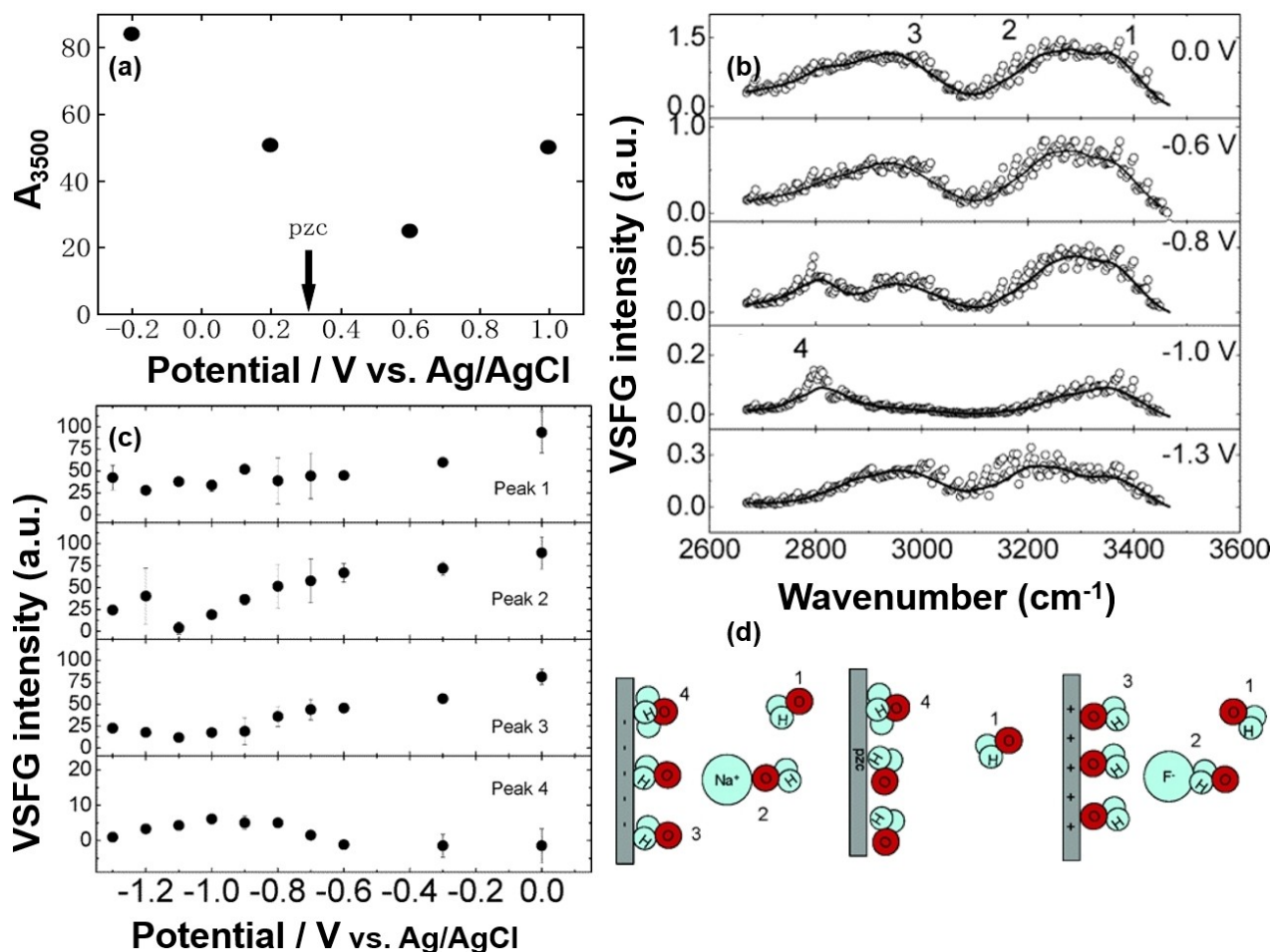


Figure 11. (a) Potential dependent VSFG amplitude at 3500 cm^{-1} (A_{3500}) of asymmetrically hydrogen-bonded relatively disordered water molecules on Au electrode in 10 mM sulfuric acid solution, showing a minimum near the point-of-zero charge. (b) VSFG spectra obtained from an Ag(1 0 0) surface in 0.1 M aqueous NaF solution at different potentials (vs. Ag/AgCl), positions of four different features are marked as 1–4 (c) Potential dependent change in intensity of those 4 peaks (d) Pictorial representation of the water orientation corresponding to four different peaks. (Figure 11a is reproduced with permission from Ref. [98], Copyright 2004 Elsevier; Figure 11b–d are reproduced with permission from Ref. [101], Copyright 2005 American Chemical Society)

on top of the broad O–H band.^[105] This sharp peak was ascribed to the existence of a non-hydrogen bonded OH group on the surface. More recently, yet another type of water structure was detected on the Au–water interface by a VSFG signal at 3680 cm^{-1} (Figure 12). This signal indicates the presence of an O–H group perpendicular to the Au surface which only interacts weakly with the Au surface, while not partaking in any hydrogen bonding.^[106] This VSFG signal resembles OH stretch features at water–hydrophobic material interface and proposed to be originated from non-hydrogen bonded O–H.^[106]

The structure of the water adlayer has also been investigated on non-metallic electrode surfaces. In an attempt to explore the potential dependence of interfacial water in an atomically thin graphene layer, Bonn and co-workers found that the graphene layer is partially transmitting the interaction between the water molecules and underlying substrates.^[107] Owing to the presence of water molecules on both sides of the graphene layer, the VSFG signal from the water molecules between the substrate and the graphene layer counteracts the signal from the water molecules on the other side of the

graphene in contact with bulk water. This leads to apparent VSFG inactivity of the free (non-hydrogen bonded) water across graphene layer. Though different aqueous interface discussed in this section cover varieties of the electrode surface in contact with it, one common realization was the influence of surface charge on the orientation of the interfacial water layer.

3.1.3. The effect of polarized electrodes

As discussed earlier, the VSFG signatures of electrode surfaces obtained under electrochemical conditions are influenced by the interfacial electric field. Such electric fields do not only alter the surface specificity of the spectroscopic method but can alter the chemistry at the interface, i.e. tune the interaction of the adsorbate and the electrode. This was observed, for example, by Schmidt et al.^[108] who applied different potentials to tune the electric field at CO/Pt (1 1 1) interface and thereby shift the Fermi level of the Pt. This caused a frequency increase and decrease in the lifetime of the C–O vibration at higher positive

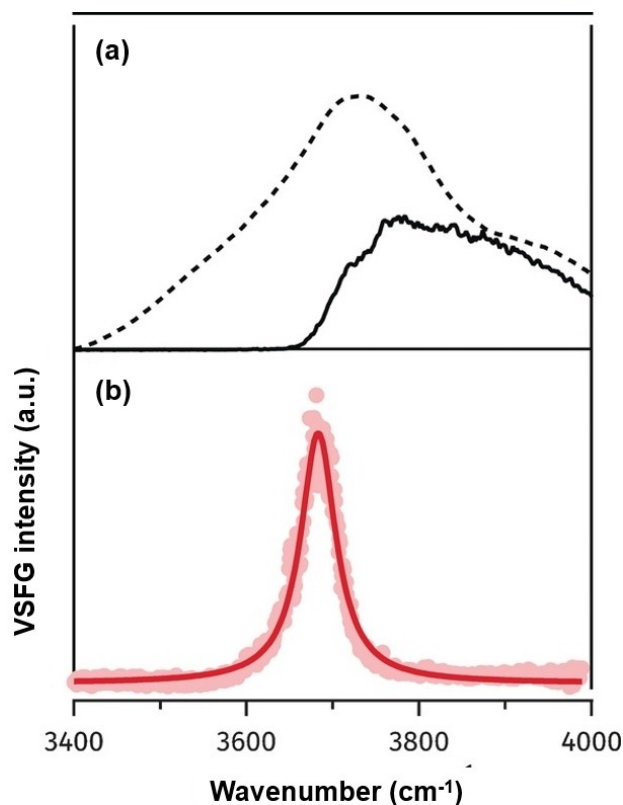


Figure 12. (a) VSFG spectrum from the Au/ aqueous HClO_4 interface at zero delays between the VIS and IR lasers, IR wavelength below 3600 cm^{-1} was absorbed by bulk water (solid line), IR beam profile (dashed line). (b) VSFG spectrum from the Au/ H_2O interface with the 800 nm beam delayed 667 fs to the IR (suppression of NR background); Lorentzian fitting indicates a peak at 3680 cm^{-1} (Reproduced with permission from Ref. [106], Copyright 2017 Wiley).

potentials as investigated by time-resolved VSFG. Such potential dependent tuning of the Fermi energy causes different resonances between the Fermi level and the electronic orbitals of the adsorbates, which in turn affects the vibrational relaxation within the adsorbates.^[109]

The influence of the electric field on the VSFG signal is more prominent when the functional group, whose vibrational mode is studied is closer to the electrode surface. Otherwise, the effect on the VSFG signal might be limited to the non-resonant response,^[110] as the latter reflects the density of occupied electronic states at the surface, which is modulated by altering the potential at the electrode surface. Hence, electrochemical VSFG spectroscopy can be used to probe the potential dependent occupation of electronic states or the distance between a molecular oscillator to the surface or interface.^[50,69] For instance, Uosaki and co-workers investigated the interaction of adsorbed CO with an underlying Pt electrode: The authors exploit the electronic resonance between the Fermi level of Pt and antibonding CO orbital to enhance the VSFG signal (Figure 13).^[111] Altering the potential shifts the Fermi energy level and the corresponding resonance energy, thus a potential-dependent study with visible pulse energy matching the energy gap could map the electronic state at the CO/Pt interface.

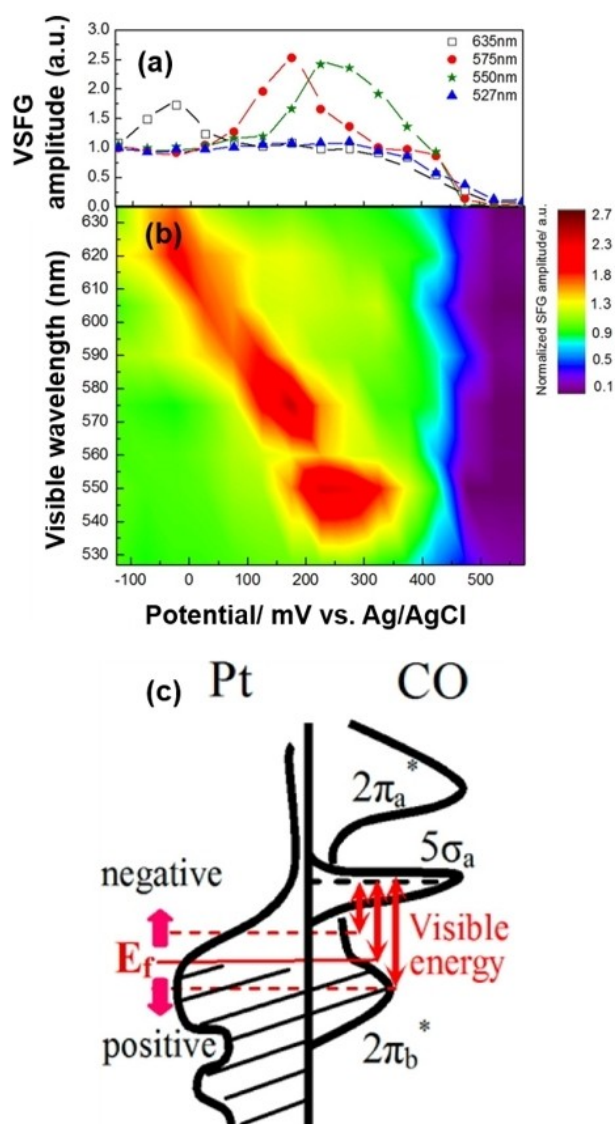


Figure 13. (a) Amplitude from the CO/Pt interface is plotted as a function of potential, visible light energy was different in each case. (b) Contour map of the VSFG amplitude as functions of the potential and wavelength of visible light. (c) Model of the electronic structure of the CO/Pt(1 1 1) electrode interface, showing the potential-induced Fermi level shift and electronic coupling of visible energy to the electronic transition between the Fermi level and antibonding 5σ state of adsorbed CO. (Reproduced with permission from Ref. [111], Copyright 2015 American Chemical Society)

Local electric fields can exist at surfaces even in absence of an applied potential. Dawlaty and co-workers implemented VSFG to probe such reaction fields at the junction of a conductor and a dielectric solvent.^[112] Their measurements involving the CN stretching frequency of 4-mercaptobenzonitrile (4-MBN) on a gold electrode in different liquid dielectric led to a theoretical model, which correlates the dielectric constant of the solvents with the interfacial reaction field and explains the redshift of the CN vibration in solvents with higher dielectric constant (Figure 14a–c). Such spectroscopic studies serving as ‘local field probes’ also exemplified that in addition to the applied potential, the ionic strength of the electrolyte influen-

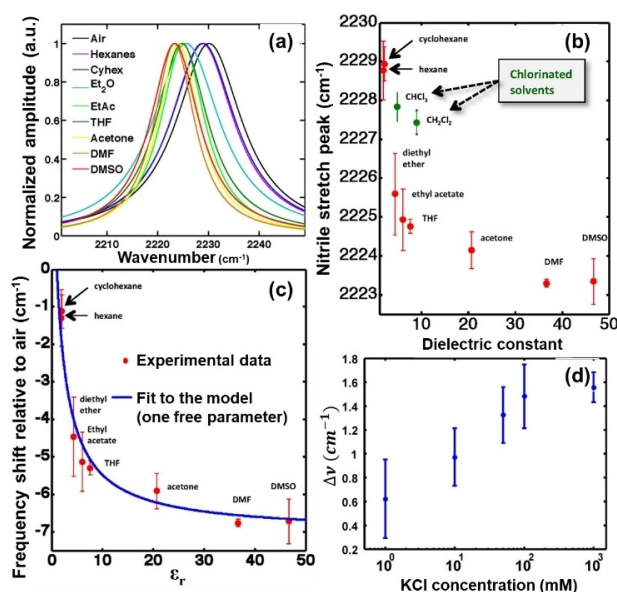


Figure 14. (a) Resonance amplitude from VSGF response of nitrile stretch from the Au-4-mercaptobenzonitrile surface in contact with a different solvent. (b) Variation of nitrile stretch peak as a function of the dielectric constant of the solvent. (c) Experimental data fitted to an Onsager-like model taking asymmetry of the interface into account (d) Frequency change as a function of ionic concentration at a fixed applied potential. (Figure 14a–c are reproduced with permission from Ref. [112], Copyright 2017 American Chemical Society, Figure 14d is reproduced from Ref. [113], Copyright 2017 American Chemical Society)

ces the electric field near the electrode. This effect was highlighted when recording the VSGF signal of CN oscillators in electrolytes with different concentrations of KCl at a fixed applied potential (Figure 1414d).^[113]

Recently this approach was further extended towards probing heterogeneous charge distribution on mineral oxide.^[114] VSGF has also been employed in combination with theoretical methods, for example, grand canonical electronic structure calculation to explore the thermodynamics of an acid dissociation reaction at varying interfacial electric field. Ge et al. probed COO⁻ vibration of 4-mercapto benzoic acid at 1400 cm⁻¹ by potential dependent VSGF measurements.^[115] Theoretically calculated pK_a values of the molecule agreed well with experimentally determined values (by comparing the VSGF amplitude of symmetric stretch of COO⁻ and phenyl ring mode) at different electric fields induced by a varying potential. The striking agreement between the experimental values and the theoretical predictions validates the findings of theoretical calculations.

3.1.4. Identifying reaction mechanism and intermediates

The application of VSGF to monitor electrochemical transformation or to detect reaction intermediates dates back to 1994 when Peremans detected a weakly bound terminal H species on a Pt electrode using in situ VSGF spectroscopy.^[116] The vibrational signature of the species appeared near

1770 cm⁻¹ irrespective of the crystallinity of the electrode surface. Based on the appearance of this band at potentials below 0 V vs. NHE, its presence can be assigned to a reaction precursor for hydrogen evolution.^[116]

However, the application of VSGF to monitor the H₂ evolution reaction has since advanced beyond the detection of adsorbed H species: Rohwerder and co-workers combined VSGF with cyclic voltammetry and ellipsometry to study the modulation of H₂ evolution rate during electrochemical desorption of a thiol monolayer.^[117] Their VSGF experiments focused on the desorption of araliphatic thiol monolayers by in situ monitoring the intensity of the pyridine ring vibration at around 1600 cm⁻¹ while scanning the potential through the region of hydrogen evolution. The authors found that even after desorption of the adsorbed monolayer, one of the araliphatic thiols preserved its two-dimensional crystallinity as suggested by the stable VSGF intensity after 10 cyclovoltammetric cycles (see Figure 15). Rohwerder proposed that immediately after the desorption of the thiols, hydrated cations get encapsulated between the suspended monolayer and negatively polarized Au electrode. This leads to an optimum pre-orientation of the water molecules for participating in the hydrogen evolution reaction (HER), thus substantially increasing the reaction rate.^[117] Methodologically, this work evidenced that not only VSGF can detect chemisorbed species on the electrode surface but rather probes the desorbed or physisorbed layers as well if those preserve their inherent ordering. A similar reductive desorption study was performed with decanethiol (DT) and octadecanethiol (ODT) SAMs on an Au electrode.^[118] With packed monolayers consisting of long alkyl chains, owing to the local inversion symmetry at the middle of a C–C bond, methylene stretching modes are usually dark in the VSGF spectrum. Induction of defects or disorders can break the inversion symmetry and thus renders such band VSGF active.^[119] At reductive potentials, the thiolate monolayers are reduced and desorb from the surface

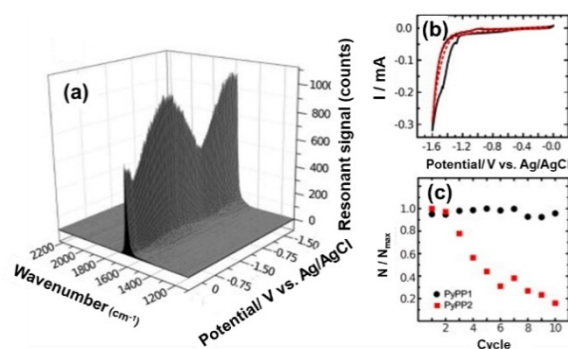


Figure 15. (a) Integrated and normalized VSGF intensities are plotted against number of voltammogram cycles. Evolution of VSGF response from pyridine ring vibration of SAMs of (4-(4-(4-pyridyl)phenyl)phenyl)methanethiol (PyPP1) on Au(1 1 1) during potential sweeps. (b) First two CV scans recorded in the SFG cell during the acquisition of spectra shown in (a). (c) Integrated SFG Intensity normalized to the maximum signal of the observed band from PyPP1/Au(1 1 1) (black circle) during ten CV cycles indicating an ordered structure, as compared to PyPP2 (red square) which shows disruption in ordered layer with increasing CV cycles (Reproduced with permission from Ref. [117], Copyright 2013 Elsevier)

leading to a decreased packing density, which benefits the formation of such defects. However, reductive desorption of DT and ODT lead to a notable difference in the VSFG response of both systems. While the methyl stretching mode from ODT remained visible at the desorption potential, indicating the presence of an ordered layer even after desorption, the respective mode was not visible at the desorption potential of the DT SAM.

Another important class of reactions that have been monitored successfully by VSFG is the electrochemical oxidation of organic acids, aldehydes, and alcohols. Electrooxidation of ethanol on a polycrystalline Pt electrode was studied in H_2SO_4 and HClO_4 .^[120] Potentiodynamic broad-band VSFG spectra indicated the adsorption of CO, $-\text{CH}_x$, CH_xO , i.e. species resulting from the ethanol oxidation at different potentials: VSFG bands at ca. 2080 and 1850 cm^{-1} confirmed the adsorption of CO on Pt both on atop and bridge sites. However, the peak at 1850 cm^{-1} , which corresponds to CO adsorbed on bridge sites, was only observed in sulfuric acid electrolyte rather than in the perchlorate electrolyte (Figure 16b). This solvent-specific adsorption of CO originates from the low CO coverage when CO is preferentially adsorbed on the Pt-bridge sites: in H_2SO_4 competitive adsorption between the (bi)sulfate anion (resulting in a VSFG band 1280 cm^{-1})^[120] and CO results in lower CO coverage.^[121] The competitive adsorption was also observed in electrochemical experiments where a lower current density was reported for ethanol oxidation in H_2SO_4 electrolyte as compared to HClO_4 electrolytes. At potentials more positive than 0.4 V vs. Ag/AgCl, oxidation of adsorbed CO leads to the disappearance of the bands indicative of CO adsorption (Figure 16a–b). At the same time removal of adsorbed CO creates vacant surface sites where adsorption of acetate occurs, which was detected in the potential range between 0.5 and 1.0 V by its characteristic IR vibration at 1410 cm^{-1} (Figure 16c), which stems from the symmetric carboxylate stretching vibration.^[122] In subsequent work on CO oxidation in alkaline media, the

authors observed a lower overpotential for CO oxidation which correlated to the disappearance of the CO peak from the VSFG spectrum at comparatively low potentials.^[123]

Adsorbed CO was also detected as a reaction intermediate during electrochemical oxidation of glycerol on a Pt electrode.^[124] In the VSFG spectra linearly bound CO species were detected at 2045–2070 cm^{-1} at potential as low as 0.05 V vs. RHE, indicating facile cleavage of C–C bond of glycerol on Pt. Upon shifting the potential from 0.05 to 0.7 V, the CO peak shifts from 2050 to 2063 cm^{-1} , a shift, that was related to alterations in the surface coverage of CO and electric field effect.^[124] At the onset of CO oxidation, the surface coverage for CO decreases, consequently weakening dipole-dipole interactions between adsorbates and ultimately causing the observed frequency shift.^[125]

These studies exemplify, that VSFG spectroscopy is well suited for detecting different adsorption modes of CO on different surface sites even in the presence of other molecules.^[120,126] Though real-time detection and assignment of linearly adsorbed or multi-bonded CO can in principle be achieved by linear vibrational spectroscopic techniques,^[127] VSFG offers the additional benefit of surface specificity. On the surface, a weakly adsorbed species can be differentiated from a chemisorbed or strongly coordinated moiety if the vibrational mode of interest is influenced by the binding. Similarly, the vibrational frequency of adsorbed CO is different from the C=O stretching frequency of carbonyl or acid. Tong et al. used this difference in probing the electrooxidation of formic acid on Pt electrode.^[128] They detected a broad and weak VSFG response at $\sim 1700 \text{ cm}^{-1}$, which is lower in frequency than adsorbed CO species. This peak originated from weakly adsorbed formic acid which is a precursor for the oxidation process. Recently, the use of in situ VSFG spectroscopy was further extended towards studying the mechanism of electrooxidation involving relatively complex molecules like 5-hydroxymethylfurfural on Nickel nitride/ carbon nanosheets.^[129]

The success of VSFG in detecting and monitoring the adsorption of CO on various electrodes inspired the use of the technique in electrochemical CO_2 reduction. In electrochemical CO_2 reduction, the adsorbed CO species (i.e., the CO molecule itself or carbonyl, carboxylate functional groups) is known to be reaction intermediate or, in multiple cases, even the final reduced product.^[130] Besides the CO_2 -reduced products, VSFG can be used to study structural changes in molecular CO_2 -reduction catalysts on surfaces. This approach was followed for example by Cowan and coworkers, who studied structural reorganization of a Mo-complex associated with the formation of the chemically active catalyst species using in-operando VSFG.^[131] The authors successfully detected the catalytically active form of the catalyst by monitoring the $\nu(\text{CO})$ modes of the Molybdenum-based metal carbonyl catalyst (Figure 17). The strong potential dependence of the $\nu(\text{CO})$ modes indicated a strong interaction of the catalytic species with the Au electrode. This interaction facilitated CO removal from the catalyst and opened a lower energy pathway for generating catalytically active species for CO_2 reduction. The authors also detected the linearly adsorbed CO directly on the

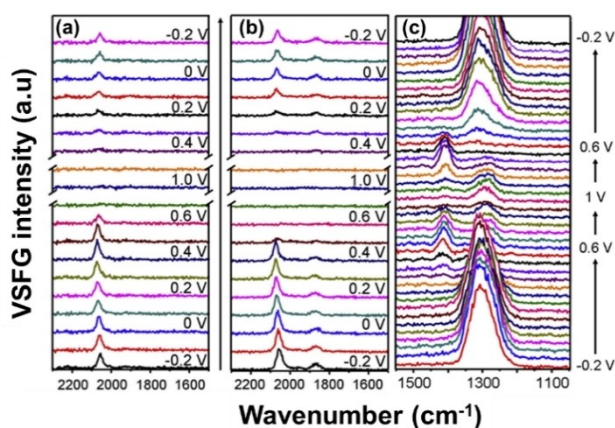


Figure 16. Potentiodynamic VSFG spectra of atop and bridge bonded CO vibrational bands recorded during 0.5 M ethanol electrooxidation on a polycrystalline Pt electrode in (a) 0.1 M HClO_4 and (b) 0.1 M H_2SO_4 . (c) (Bi)sulfate and adsorbed acetate (at $E > 0.6 \text{ V}$ vs. Ag/AgCl) vibrational bands (0.1 M H_2SO_4) appears above the NR background at potentials (Reproduced with permission from Ref. [120], Copyright 2011 Elsevier)

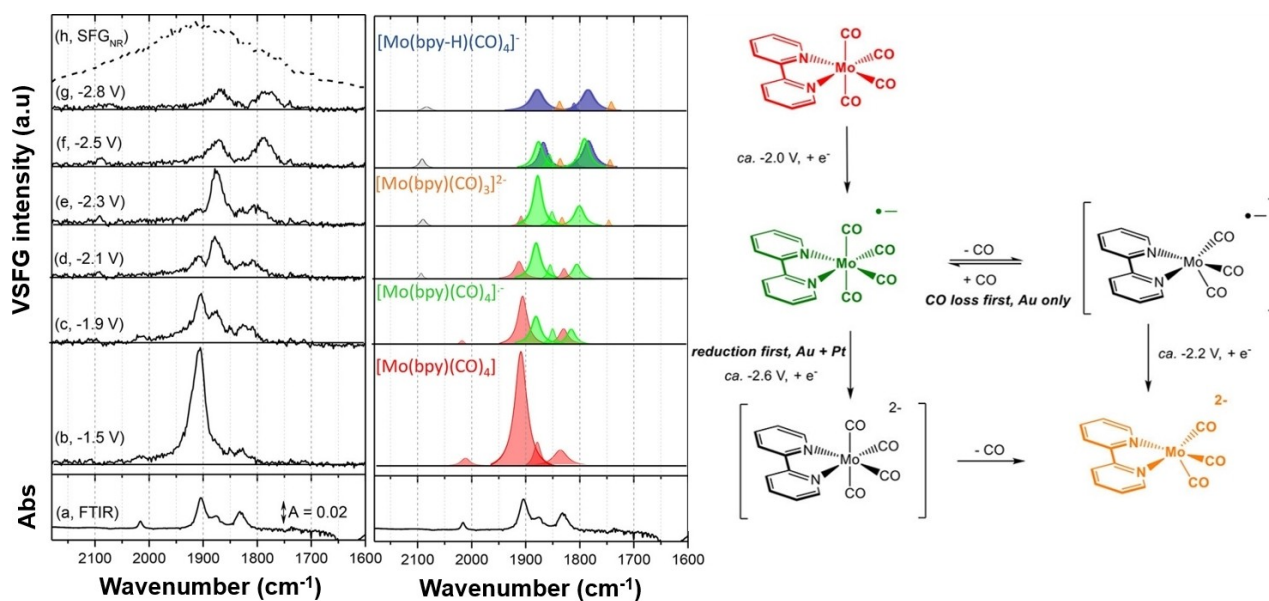


Figure 17. Solution phase FTIR (a) and in situ VSG spectra (b–g) of $[\text{Mo}(\text{bpy})(\text{CO})_4]$ at an Au electrode in CH_3CN and 0.1 M TBAPF_6 under Ar. The FTIR spectrum is recorded at open circuit potential and the VSG spectra at different potentials as indicated. The intensity of the NR background (dashed line, h) of the cell recorded with 0 ps time-delay between the IR and 800 nm laser pulses provides an approximation of the spectrum of the broadband IR pulse. Spectra (b–g) are recorded with a 0.45 ps delay between the IR and asymmetric 800 nm laser pulses. Center: a pictorial representation of the proposed assignments. The assignments at -2.3 and -2.5 V are tentative due to the presence of a complex mixture of species (≥ 3) with spectral features at similar positions. The gray VSG peak at ca. 2090 cm^{-1} is due to CO at the gold electrode, the purple peaks are assigned to $[\text{Mo}(\text{bpy-H})(\text{CO})_4]^-$. Right: Scheme showing the proposed mechanisms for the formation of active catalytic form. (Reproduced with permission from Ref. [131], <https://pubs.acs.org/doi/10.1021/jacs.7b06898>, Copyright 2017 American Chemical Society, further permissions related to the material should be directed to the ACS)

Au electrode by its characteristic vibrational signature at 2090 cm^{-1} . The behavior differed from CO_2 reduction on a Pt electrode, where only a weak potential dependency was reported. Following a similar approach, the same group followed the formation of different CO_2 reduction intermediate using a $[\text{Mn}(\text{bpy})(\text{CO})_3\text{Br}]$ electrocatalyst.^[126b] From the operando VSG data in the absence of CO_2 , they inferred hydride intermediates, which were not present under CO_2 atmosphere.

VSG bands at 1976 , 1875 , and 1600 cm^{-1} were assigned to reaction intermediates involving metal carbonyls binding the reduced CO_2 species in different geometries. Introducing isotopically labeled CO_2 , i.e. $^{13}\text{C}^{18}\text{O}_2$, enabled the assignment of individual vibrational modes in the VSG spectrum. On a different note, Wang and co-workers probed the products from electrochemical CO_2 reduction on Au and Cu electrodes.^[132] On the Au electrode, the VSG response at 2100 cm^{-1} showed linear adsorption of CO. The vibrational mode exhibited a strong Stark shift of $44.4\text{ cm}^{-1}\text{ V}^{-1}$ in the potential range of -0.5 to -1.3 V vs. SCE. The assignment of linearly adsorbed CO on Au electrode was in line with previously reported IR spectroscopic data.^[133] However, the spectroscopic findings on the Cu electrode pointed to a different interaction mechanism at the surface: The absence of any resonance VSG response in the same potential window suggested either a random orientation of CO species and/or an ultra-short lifetime of the adsorbed CO. Nevertheless, on the Cu electrode, the orientation of the adsorbed CO favors the formation of C–C bond, indicated by the observation of the asymmetric C–H stretching of methyl

and methylene groups of a surface ethoxy moiety ($\text{Cu-OCH}_2\text{-CH}_3$) at 2996 and 2936 cm^{-1} .^[132]

3.1.5. Vibrational relaxation dynamics in molecularly functionalized electrodes

To study vibrational dynamics in the CO_2 reduction catalysts $\text{Re}(\text{dcbpy})(\text{CO})_3\text{Cl}$ (ReCO A) [$\text{dcbpy} = 2,2'$ -bipyridine- $4,4'$ -(COOH) $_2$] immobilized on a Au surface, time-resolved broadband VSG (TR-VSG) proved successful.^[134] Following vibrational excitation by IR pump pulse, the temporally delayed VSG pulse sequence served as a probe of the molecular structural changes in the complex.

Excitation of the molecules occurred at 2025 cm^{-1} , i.e. in resonance with the symmetric CO stretch vibration.^[135] The resulting TR-VSG spectrum of adsorbed catalyst showed ground state bleaching at 2025 cm^{-1} and excited-state absorption at 2005 cm^{-1} (Figure 18). From the (bi-exponential) decay kinetics, a rapidly populated equilibrium between the CO stretching modes by intramolecular vibrational energy relaxation was identified as a key relaxation step. In a comprehensive VSG spectroscopic study coupled with theoretical calculation, Lian, Batista, Kubiak, and co-workers elucidated the structural influence of a Rhenium catalyst (for CO_2 reduction reaction) on adsorbate-substrate interaction and interfacial energy transfer.^[136] Authors highlighted the requirement of new anchoring (immobilization of the catalyst on electrode) strategies, as at potentials more negative than -1.0 V vs. Ag/AgCl ,

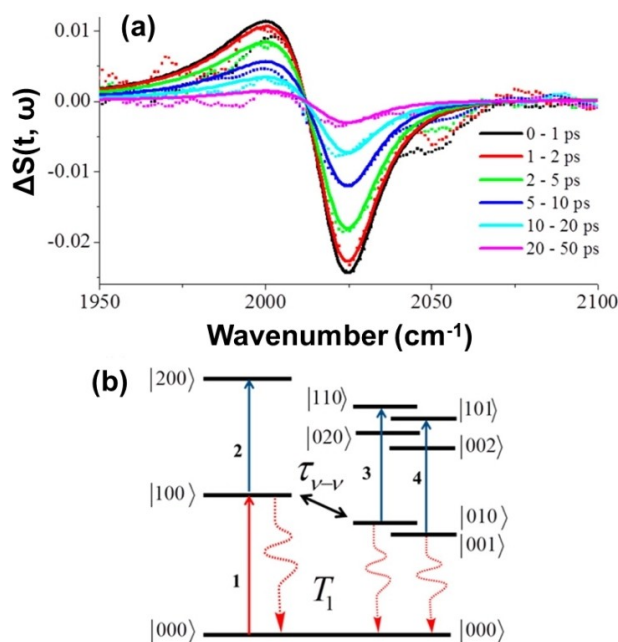


Figure 18. (a) Normalized TR-VSFG difference spectra of ReCO-Au recorded at different pump-VSFG delays as indicated in the figure. (b) Vibrational energy level scheme of the coupled CO stretching modes of ReCO A-type complexes. (Reproduced with permission from Ref. [134], Copyright 2012 American Chemical Society)

desorption of catalysts inhibited VSFG probing of the catalyst in action.^[136]

3.2. Solid electrolyte interfaces in Li-ion batteries

Li-ion batteries represent the state-of-the-art benchmark in the field of rechargeable batteries.^[137] Various spectroelectrochemical techniques are key in elucidating the physical and chemical processes occurring at electrodes of Li-ion batteries.^[79b] Realization of VSFG on the electrode-electrolyte interface opened the possibility to directly probe the interfacial phenomena in operando and to selectively monitor the dynamics at the solid-electrolyte interphase.^[138] In the following, we summarize the use of VSFG to study solvent adsorption, the formation of solid electrolyte interphase, and potential induced surface modification of the electrode (Li deposition/stripping).

3.2.1. VSFG applied to study cathode surfaces

The first implementation of VSFG in the field of Li-ion batteries focused on the adsorption of linear and cyclic alkyl carbonates, popular electrolyte additives for Li-ion batteries, on a LiCoO₂ cathode. Ye and co-workers realized VSFG in an internal reflection geometry after depositing a thin film of LiCoO₂ on a CaF₂ prism.^[139] Bringing the cathode surface in contact with the propylene carbonate (PC) electrolyte, the vibrational resonance response of $\nu(\text{C}=\text{O})$ indicated two different orientations of the

adsorbed PC (see Figure 19). In presence of multiple alkyl carbonates in the electrolyte, preferential adsorption of cyclic ethylene carbonate (EC) over linear diethyl carbonate (DEC) and dimethyl carbonate (DMC) was reported.^[140] In all these VSFG spectra two resonant responses were identified, which originated from differently oriented molecules at the interface. Polarization-dependent VSFG experiments revealed the tilt angle of the C=O group (of adsorbed EC) as 12° and 171°, which confirms the existence of two different orientations of EC and thus different extent of interaction between C=O group and electrode surface.^[140] A redshift in frequency was observed in the C=O mode of adsorbed EC pointing towards the electrode surface due to its relatively stronger interaction with LiCoO₂. Though these studies were performed under open-circuit conditions, important information about adsorption and orientation of the electrolyte molecules were obtained.

3.2.2. VSFG applied to study anode surfaces

The adsorption of carbonate solvents was also studied on anode surfaces. Peng et al. observed preferential adsorption of PC molecules over DMC on a carbon substrate by two distinct VSFG signals stemming from C=O groups pointing towards and away from the anode surface.^[54]

However, the focus of VSFG experiments on anode surfaces was on the formation of the solid electrolyte interphase (SEI) which determines the long-term stability and cyclability of Li-ion batteries. SEI is generated in the first few charging cycles of the battery by decomposition of the electrolytes.^[141] The very first application of in situ VSFG targeting SEI formation was conducted with Cu and Au electrodes.^[142] Formation of the SEI upon scanning the voltage from 2.0 V to 0.2 V (vs. Li/Li⁺) generates two interfaces, an electrode/SEI interface, and an SEI/electrolyte interface. Upon changing the potential, the position of the electrode/SEI interface remains fixed (in space) but due to the shrinking of SEI, the SEI/electrolyte interface moves periodically in the lab frame. The variable thickness of SEI causes an optical interference effect between the reflected and transmitted (eventually reflected from electrode surface) VSFG signal of ethylene carbonate (EC) from the electrolyte/SEI interface. This contributes to the potential dependency of the VSFG signal stemming from the EC molecules. As noted by the authors, potential driven reorientation of EC molecules were present on both Au and Cu electrode, however, the influence of optical interference on the VSFG signal was realized only with Cu electrode. On the Au electrode, such effect was not observed due to the comparably opaque SEI formed on the latter metal.

Clott and coworkers pointed out that care has to be taken in interpreting VSFG signals stemming from an electrode/SEI interface. Using a model anodic half cell with an Au electrode, Clott observed that the IR pulse, the intensity of which is attenuated in specific frequency ranges due to absorption from the electrolyte, can produce illusory or 'phantom' SFG signals.^[143] To rationalize their experimental results, Clott and coworkers suggested a model that considers both second ($\chi^{(2)}$)

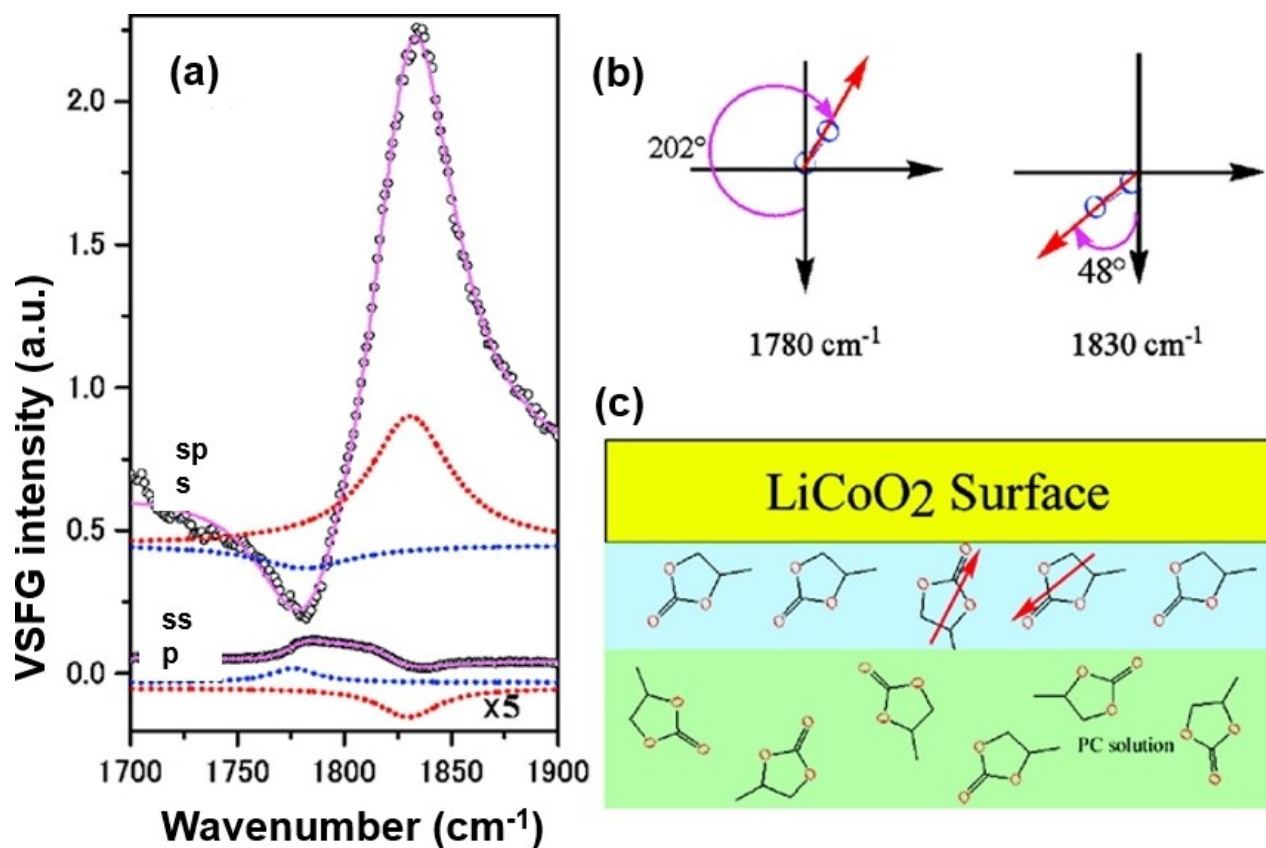


Figure 19. (a) *sps*- and *ssp*-VSFG spectra (circles) of LiCoO₂ surface in contact with PC. VSFG spectra are offset for clarity. Red and blue dotted lines are simulated components corresponding to two orientations of the C=O group as shown in (b). (c) Schematic illustration of PC absorption on LiCoO₂ surface. (Reproduced with permission from Ref. [139], Copyright 2009 American Chemical Society)

and third-order ($\chi^{(3)}$) susceptibilities. Their observations suggest that in presence of a large electric field, the potential dependency of the VSFG signal has a significant contribution from the third-order term [$\chi^{(3)} \times E_{VIS}(\omega_1) \times E_{IR}(\omega_2) \times E_{DC}$] (see Equation (3)). In these calculations, both second ($\chi^{(2)}$) and third-order ($\chi^{(3)}$) susceptibilities were considered potential independent. However, Li deposition and stripping at the anode (Au) affects the nonlinear effects on the surface and cause changes in the VSFG response originating from the electrode surface at the respective potentials. This provides direct means to monitor Li deposition or Li stripping from the electrode, even though Li ions themselves do not have vibrational resonances in the mid-IR range. Unlike the VSFG on electrode surface, signals from the SEI was not influenced by the Li deposition or stripping, instead, the evolution of the SEI during individual charging/discharging cycles was monitored by the VSFG response stemming from constituents of the SEI, for example Lithium ethylene dicarbonate (LiEDC).

Horowitz et al. studied the reduction of an EC/DEC solvent on crystalline silicon electrodes in a Li-ion battery half cell system.^[144] From the operando VSFG signal, the authors concluded about the formation of a Si-ethoxy species, which is associated with the vibrational mode $-\text{CH}_3$ and $-\text{OCH}_2$ detected at a potential of about 1 V (vs. Li/Li⁺) (see Figure 20).

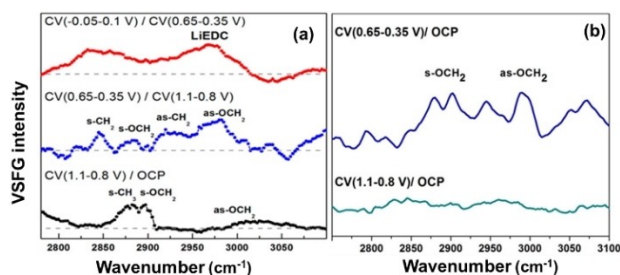


Figure 20. (a) VSFG intensity (divided by another SFG response during CV at the particular potential range or OCP) under reaction conditions from crystalline silicon Si(1 0 0)-hydrogen-terminated anode in contact with EC/DEC. At 1.1 V \rightarrow 0.8 V (vs. Li/Li⁺) evolution of the peak near 2895 cm⁻¹ corresponds to the s-OCH₂ group stretch associated with the Si-ethoxy formation. Which is not seen in presence of only EC (b) (Reproduced with permission from Ref. [144], Copyright 2016 American Chemical Society)

Corresponding vibrational features were only visible in the presence of DEC and with H terminated Si. Therefore, the authors proposed a mechanism, that involved the formation of an ethoxy radical (or anion) which reacts with acidic Si sites leading to the formation of a Si-ethoxy bond. EC does not allow for this reaction to proceed as the corresponding anion of EC will lead to the formation of LiEDC.

Additional VSFG experiments addressed the mechanism of DEC decomposition, which starts even at open circuit potential (OCP) when the electrolyte is in contact with an acidic silicon surface.^[145] However, it was reported earlier that the use of fluorinated electrolytes increases the stability of the SEI^[146] and improves cyclability.^[147] Comparative VSFG studies of the electrode/SEI interface formed by 1,2-diethoxy ethane and its fluorinated version on Si anode indicated that using the fluorinated electrolyte increases the ordering of the interface and leads to narrower and more intense VSFG bands. The underlying mechanism was associated with changes in the orientation of the $-\text{CF}_3$ end groups of linear fluorinated ether with respect to the surface. While working with a cyclic carbonate (EC) and its fluorinated form (FEC) on silicon and sapphire surfaces, Horowitz et al. observed a similar reorientation with more FEC rich solvent.^[148] They conducted VSFG experiments with different polarization geometries to probe the orientation of the $\text{C}=\text{O}$ oscillator (see Figure 21). Their experimental results indicated that the oscillators are preferentially oriented perpendicularly to the surface upon addition of FEC. This FEC induced ordering might be helpful for Li^+ ion diffusion through the electrolyte molecules, as indicated by the authors. Successive VSFG experiments and additional theoretical studies revealed that upon adsorption of EC or FEC, the strong $\text{Si}-\text{O}$ bond inhibits desorption of EC/FEC.^[149] Olson et al. conducted further studies in this direction with nano particle-based Si electrodes. Their observation suggests that electrochemical reduction of the EC on lithiated Si nanoparticles produces soluble and unstable byproducts, which readily diffuse from the interface as indicated by the absence of SFG signals.^[150] On the other hand, potential-dependent reduction of FEC produced

LiF , Li_2CO_3 , fluorinated alkyl species thus suppressing the generation of soluble constituents in the SEI.

4. Conclusion

This review discusses the development of VSFG spectroscopy as an operando spectroscopic technique to study electrochemical interface. In particular, the combination of VSFG spectroscopy with electrochemical methods proved successful in unraveling molecular processes underlying the overall electrochemical process at the surface or interface. For instance, knowledge gained from studying adsorption and reorientation of small molecules, for example CO or nitriles, formed the basis for studying complex molecular catalysts at interfaces. Potential-controlled VSFG experiments revealed the response of interfacial molecular layers to changes in the surface charge or surface electric fields. While it is important to realize the different effects caused by changes in molecular dipole moment, polarizability, or its physical orientation when subjected to an external electric field or internal reaction field, the specific assignment/quantification of these effects in VSFG response poses significant challenges. Hence complementary theoretical studies have been established as the gold standard, which themselves are however not the focus of this review.

Analyzing the current trends and results from VSFG experiments targeting different electrochemical systems, we highlight the success of VSFG in detecting adsorbed species, in tracking adsorbate orientation at surfaces, and in monitoring the real-time surface reaction. The extent of electrode-catalyst interaction is also realized by monitoring the stark shift of the adsorbed species. The application of this technique in observing the electrochemical phenomena in battery half-cell provides information regarding the solvent adsorption process. Also, in presence of different electrolytes/electrodes, different components in the formation and dynamics of the SEI was explored.

At the current stage, VSFG is arguably one of the most effective spectroscopic technique to study solid-electrolyte interface under operando conditions. However, the complex and dynamic nature of the electrode-electrolyte interface for example in energy storage devices makes the interpretation of the data challenging. Active collaboration between spectroscopy (VSFG) and material chemistry or energy research is certainly an asset in modelling such function-determining interfaces in energy storage devices. As our understanding of these interfaces improves, a broader and more general use of VSFG in energy research is expected. For analyzing the data more quantitatively development of theoretical studies with comparable systems will also be useful.

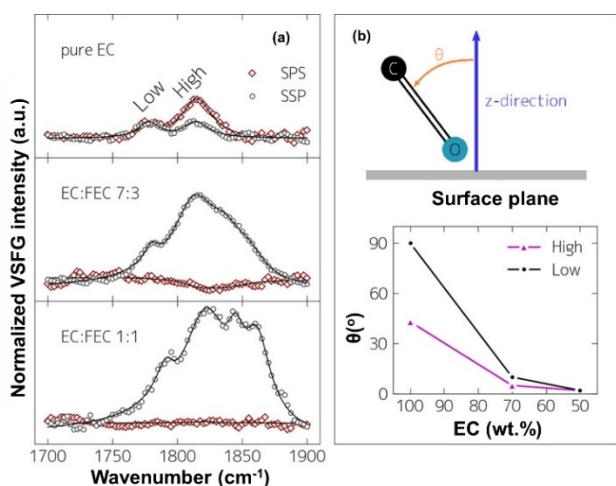


Figure 21. (a) VSFG spectra of EC/FEC mixtures at a different ratio at open circuit potential probed at *ssp* (open circles) and *sps* (open diamonds) polarization. In the top left panel “low” and “high” are assigned to vibration of EC carbonyl group with tight and loosely packed molecules respectively. (b) Top, an illustration showing the $\text{C}=\text{O}$ vector and its angle (θ) from the normal to the surface. Bottom, the $\text{C}=\text{O}$ bond angle to the surface normal as a function of FEC wt % content. (Reproduced with permission from Ref. [148], Copyright 2018 American Chemical Society)

Acknowledgments

Financial support of the Carl-Zeiss-Foundation via the Durchbrüche-Programm (project Intelligente Substrate: Schaltbare Grenzflächen auf Basis multiresponsiver Hybridmaterialien) is

greatly acknowledged. Open Access funding enabled and organized by Projekt DEAL.

Conflict of Interest

The authors declare no conflict of interest.

Keywords: electrochemical interface · interfacial electric field · Li-ion battery · vibrational sum frequency generation spectroscopy · surface reaction

- [1] a) C. G. Vayenas, *J. Solid State Electrochem.* **2011**, *15*, 1425–1435; b) E. Santos, W. Schmickler, *Catalysis in electrochemistry: from fundamental aspects to strategies for fuel cell development*, Vol. 7, John Wiley & Sons, **2011**.
- [2] G. Hilt, *ChemElectroChem* **2020**, *7*, 395–405.
- [3] L. Janssen, L. Koene, *Chem. Eng. J.* **2002**, *85*, 137–146.
- [4] a) H. Ibrahim, A. Ilinca, J. Perron, *Renewable Sustainable Energy Rev.* **2008**, *12*, 1221–1250; b) B. G. Pollet, I. Staffell, J. L. Shang, *Electrochim. Acta* **2012**, *84*, 235–249.
- [5] I. Katsounaros, S. Cherevko, A. R. Zeradjanin, K. J. Mayrhofer, *Angew. Chem. Int. Ed.* **2014**, *53*, 102–121; *Angew. Chem.* **2014**, *126*, 104–124.
- [6] a) J.-S. Wei, T.-B. Song, P. Zhang, X.-Q. Niu, X.-B. Chen, H.-M. Xiong, *Mater. Chem. Front.* **2020**, *4*, 729–749; b) W. Guo, Y. Meng, Y. Hu, X. Wu, Z. Ju, Q. Zhuang, *Front. Energy Res.* **2020**, *170*; c) D. L. T. Nguyen, Y. Kim, Y. J. Hwang, D. H. Won, *Carbon Energy.* **2020**, *2*, 72–98.
- [7] a) J. M. Bockris, M. Devanathan, K. Müller, *Electrochemistry*, Elsevier, **1965**, pp. 832–863; b) L. Blum, *J. Phys. Chem.* **1977**, *81*, 136–147; c) W. Schmickler, D. Henderson, *Prog. Surf. Sci.* **1986**, *22*, 323–419.
- [8] G. Gonella, E. H. Backus, Y. Nagata, D. J. Bonthuis, P. Loche, A. Schlaich, R. R. Netz, A. Kühnle, I. T. McCrum, M. Koper, *Nat. Chem. Rev.* **2021**, *5*, 466–485.
- [9] P. Christensen, A. Hamnet, *Techniques and mechanisms in electrochemistry*, Springer Science & Business Media, **2007**.
- [10] a) D. Fraggedakis, M. Z. Bazant, *J. Chem. Phys.* **2020**, *152*, 184703; b) S. H. Chang, N. Danilovic, K.-C. Chang, R. Subbaraman, A. P. Paulikas, D. D. Fong, M. J. Highland, P. M. Baldo, V. R. Stamenkovic, J. W. Freeland, *Nat. Commun.* **2014**, *5*, 1–9.
- [11] M. A. Bos, Z. Shervani, A. C. Anusium, M. Giesbers, W. Norde, J. M. Kleijn, *Colloids Surf. B* **1994**, *3*, 91–100.
- [12] a) K.-i. Ataka, T. Yotsuyanagi, M. Osawa, *J. Phys. Chem.* **1996**, *100*, 10664–10672; b) X. Li, A. A. Gewirth, *J. Am. Chem. Soc.* **2003**, *125*, 11674–11683.
- [13] a) J. Lück, A. Latz, *Phys. Chem. Chem. Phys.* **2018**, *20*, 27804–27821; b) M. Dunwell, Y. Yan, B. Xu, *Curr. Opin. Chem. Eng.* **2018**, *20*, 151–158.
- [14] L. A. Dick, A. J. Haes, R. P. Van Duyne, *J. Phys. Chem. B.* **2000**, *104*, 11752–11762.
- [15] N. Bartels, K. Golibrzuch, C. Bartels, L. Chen, D. J. Auerbach, A. M. Wodtke, T. Schäfer, *Proc. Nat. Acad. Sci.* **2013**, *110*, 17738–17743.
- [16] O. M. Magnussen, *Eur. J. Chem.* **2019**, *25*, 12865–12883.
- [17] E. L. Clark, S. Ringe, M. Tang, A. Walton, C. Hahn, T. F. Jaramillo, K. Chan, A. T. Bell, *ACS Catal.* **2019**, *9*, 4006–4014.
- [18] T. Iwasita, H. Hoster, A. John-Anacker, W. Lin, W. Vielstich, *Langmuir* **2000**, *16*, 522–529.
- [19] M. Liu, Y. Pang, B. Zhang, P. De Luna, O. Voznyy, J. Xu, X. Zheng, C. T. Dinh, F. Fan, C. Cao, *Nature* **2016**, *537*, 382–386.
- [20] a) K. Chan, J. K. Nørskov, *J. Phys. Chem. Lett.* **2016**, *7*, 1686–1690; b) A. B. Anderson, *J. Electroanal. Chem. Interfacial Electrochem.* **1990**, *280*, 37–48.
- [21] a) J. Wandt, P. Jakes, J. Granwehr, R.-A. Eichel, H. A. Gasteiger, *Mater.* **2018**, *21*, 231–240; b) H. Arnolds, M. Bonn, *Surf. Sci. Rep.* **2010**, *65*, 45–66.
- [22] R. R. Unocic, K. L. Jungjohann, B. L. Mehdi, N. D. Browning, C. Wang, *MRS Bull.* **2020**, *45*, 738–745.
- [23] a) J. Y. Park, *Charact. Mater.* **2002**, 1–10; b) C. R. So, C. Tamerler, M. Sarikaya, *Angew. Chem. Int. Ed.* **2009**, *48*, 5174–5177; *Angew. Chem.* **2009**, *121*, 5276–5279.
- [24] a) K. Borgwarth, C. Ricken, D. Ebling, J. Heinze, *Ber. Bunsen-Ges.* **1995**, *99*, 1421–1426; b) R. C. Engstrom, C. M. Pharr, *Anal. Chem.* **1989**, *61*, 1099 A–1104 A.
- [25] A. K. Yagati, J. Min, J.-W. Choi, *Mod. Electrochem. Methods Nano. Surf. Corros. Sci.* **2014**, *55*.
- [26] a) L. Rakočević, S. Štrbac, I. Srejić, *Int. J. Hydrogen Energy.* **2021**, *46*, 9052–9063; b) D. Weingarth, A. Foelske-Schmitz, A. Wokaun, R. Kötz, *Electrochem. Commun.* **2011**, *13*, 619–622.
- [27] E. A. Carbonio, J.-J. Velasco-Velez, R. Schlögl, A. Knop-Gericke, *J. Electrochem. Soc.* **2020**, *167*, 054509.
- [28] D. J. Aberdam in *Spectroscopic and Diffraction Techniques in Interfacial Electrochemistry*, (Eds: C. Gutiérrez, C. Melendres) vol 320, Springer, Dordrecht, **1990**, pp. 383–407.
- [29] H. Ali-Löyty, M. W. Louie, M. R. Singh, L. Li, H. G. Sanchez Casalongue, H. Ogasawara, E. J. Crumlin, Z. Liu, A. T. Bell, A. Nilsson, *J. Phys. Chem. C* **2016**, *120*, 2247–2253.
- [30] a) M. Zhao, Y. Gu, W. Gao, P. Cui, H. Tang, X. Wei, H. Zhu, G. Li, S. Yan, X. Zhang, *Appl. Catal. B* **2020**, *266*, 118625; b) R. De, S. Gonglach, S. Paul, M. Haas, S. Sreejith, P. Gerschel, U. P. Apfel, T. H. Vuong, J. Rabeah, S. Roy, *Angew. Chem. Int. Ed.* **2020**, *132*, 10614–10621.
- [31] V. Shutthanandan, M. Nandasiri, J. Zheng, M. H. Engelhard, W. Xu, S. Thevuthasan, V. Murugesan, *J. Electron Spectrosc. Relat. Phenom.* **2019**, *231*, 2–10.
- [32] A. J. Keeler, G. R. Salazar-Banda, A. E. Russell, *Curr. Opin. Electrochem.* **2019**, *17*, 90–96.
- [33] H. Seki, K. Kunimatsu, W. Golden, *Appl. Spectrosc.* **1985**, *39*, 437–443.
- [34] C. Smith, A. Bowfield, G. Dolan, M. Cuquerella, C. Mansley, D. Fernig, C. Edwards, P. Weightman, *J. Chem. Phys.* **2009**, *130*, 044702.
- [35] N. Heidary, N. Kornienko, *Chem. Commun.* **2020**, *56*, 8726–8734.
- [36] J. Zeng, D.-i. Jean, C. Ji, S. Zou, *Langmuir* **2012**, *28*, 957–964.
- [37] Y.-J. Zhang, Z.-F. Su, J.-F. Li, J. Lipkowski, *J. Phys. Chem. C.* **2020**, *124*, 13240–13248.
- [38] S. Hy, Y.-H. Chen, J.-y. Liu, J. Rick, B.-J. Hwang, *J. Power Sources* **2014**, *256*, 324–328.
- [39] a) Q. Cheng, L. Wei, Z. Liu, N. Ni, Z. Sang, B. Zhu, W. Xu, M. Chen, Y. Miao, L.-Q. Chen, *Nat. Commun.* **2018**, *9*, 1–10; b) Q. Cheng, Y. Miao, J. Wild, W. Min, Y. Yang, *Matter* **2021**, *4*, 1460–1483.
- [40] C. L. Haynes, A. D. McFarland, R. P. Van Duyne, *Anal. Chem.* **2005**, *77*, 338 A–346 A.
- [41] H.-F. Wang, W. Gan, R. Lu, Y. Rao, B.-H. Wu, *Int. Rev. Phys. Chem.* **2005**, *24*, 191–256.
- [42] a) A. Sayama, S. Nihonyanagi, Y. Ohshima, T. Tahara, *Phys. Chem. Chem. Phys.* **2020**, *22*, 2580–2589; b) N. Ji, V. Ostroverkhov, C.-Y. Chen, Y.-R. Shen, *J. Am. Chem. Soc.* **2007**, *129*, 10056–10057.
- [43] A. G. Lambert, P. B. Davies, D. J. Neivandt, *Appl. Spectrosc. Rev.* **2005**, *40*, 103–145.
- [44] a) A. Morita, in *Theory of Sum Frequency Generation Spectroscopy*, Vol. 35, Springer, Singapore, **2018**; b) Y. Shen, in *Fundamentals of sum-frequency spectroscopy*, Cambridge University Press, **2016**.
- [45] I. V. Stioptkin, H. D. Jayathilake, A. N. Bordenyuk, A. V. Benderskii, *J. Am. Chem. Soc.* **2008**, *130*, 2271–2275.
- [46] A. J. Moad, G. J. Simpson, *J. Phys. Chem. B* **2004**, *108*, 3548–3562.
- [47] N. G. Rey, D. D. Dlott, *J. Electroanal. Chem.* **2017**, *800*, 114–125.
- [48] C. M. Lee, K. Kafle, S. Huang, S. H. Kim, *J. Phys. Chem. B* **2016**, *120*, 102–116.
- [49] G. Lu, A. Lagutchev, D. D. Dlott, A. Wieckowski, *Surf. Sci.* **2005**, *585*, 3–16.
- [50] A. Ge, P. E. Videla, G. L. Lee, B. Rudshiteyn, J. Song, C. P. Kubiak, V. S. Batista, T. Lian, *J. Phys. Chem. C* **2017**, *121*, 18674–18682.
- [51] A. Ge, K.-i. Inoue, S. Ye, *J. Chem. Phys.* **2020**, *153*, 170902.
- [52] N. G. Rey, D. D. Dlott, *Phys. Chem. Chem. Phys.* **2017**, *19*, 10491–10501.
- [53] L. Yu, H. Liu, Y. Wang, N. Kuwata, M. Osawa, J. Kawamura, S. Ye, *Angew. Chem. Int. Ed.* **2013**, *125*, 5865–5868.
- [54] Q. Peng, H. Liu, S. Ye, *J. Electroanal. Chem.* **2017**, *800*, 134–143.
- [55] A. Ge, D. Zhou, K.-i. Inoue, Y. Chen, S. Ye, *J. Phys. Chem. C* **2020**, *124*, 17538–17547.
- [56] W.-T. Liu, Y. R. Shen, *Proc. Nat. Acad. Sci.* **2014**, *111*, 1293–1297.
- [57] Z. Liu, Y. Li, Q. Xu, H. Wang, W.-T. Liu, *J. Phys. Chem. Lett.* **2019**, *11*, 243–248.
- [58] S. Wallentine, S. Bandaranayake, S. Biswas, L. R. Baker, *J. Phys. Chem. A* **2020**, *124*, 8057–8064.
- [59] P. Guyot-Sionnest, A. Tadjeddine, *Chem. Phys. Lett.* **1990**, *172*, 341–345.
- [60] a) J. Bénard, *Adsorption on Metal Surfaces: An Integrated Approach*, (Eds: J. Bénard) Elsevier, **1983**; b) J. Lipkowski, L. Stolberg, D.-F. Yang, B.

- Pettinger, S. Mirwald, F. Henglein, D. Kolb, *Electrochim. Acta* **1994**, *39*, 1045–1056; c) J. Moiroux, P. J. Elving, *Anal. Chem.* **1978**, *50*, 1056–1062.
- [61] D. Bohra, I. Ledezma-Yanez, G. Li, W. de Jong, E. A. Pidko, W. A. Smith, *Angew. Chem. Int. Ed.* **2019**, *58*, 1345–1349; *Angew. Chem.* **2019**, *131*, 1359–1363.
- [62] J. Chen, L. Fang, S. Luo, Y. Liu, S. Chen, *J. Phys. Chem. C* **2017**, *121*, 6209–6217.
- [63] Y.-P. Sun, K. Scott, *Chem. Eng. J.* **2004**, *102*, 83–91.
- [64] Y.-G. Zhou, B. Haddou, N. V. Rees, R. G. Compton, *Phys. Chem. Chem. Phys.* **2012**, *14*, 14354–14357.
- [65] D. M. Kolb, *Angew. Chem. Int. Ed.* **2001**, *40*, 1162–1181; *Angew. Chem.* **2001**, *113*, 1198–1220.
- [66] C. Hess, M. Wolf, M. Bonn, *Phys. Rev. Lett.* **2000**, *85*, 4341.
- [67] A. Tadjeddine, A. Peremans, P. Guyot-Sionnest, *Surf. Sci.* **1995**, *335*, 210–220.
- [68] A. Tadjeddine, A. Le Rille, O. Pluchery, F. Vidal, W. Q. Zheng, A. Peremans, *Phys. Status Solidi A* **1999**, *175*, 89–107.
- [69] A. Tadjeddine, F. Vidal, in *In Situ Spectroscopic Studies of Adsorption at the Electrode and Electrocatalysis*, (Eds: S. G. Sun, P. A. Christensen, A. Wieckowski) Elsevier, **2007**, 273–298.
- [70] S. A. Swanson, R. McClain, K. S. Lovejoy, N. B. Alamdari, J. S. Hamilton, J. C. Scott, *Langmuir* **2005**, *21*, 5034–5039.
- [71] F. Vidal, B. Busson, C. Six, A. Tadjeddine, L. Dreesen, C. Humbert, A. Peremans, P. Thiry, *J. Electroanal. Chem.* **2004**, *563*, 9–14.
- [72] F. Vidal, B. Busson, A. Tadjeddine, *Chem. Phys. Lett.* **2005**, *403*, 324–328.
- [73] D. K. Lambert, *Electrochim. Acta* **1996**, *41*, 623–630.
- [74] B. Persson, R. Ryberg, *Phys. Rev. B* **1981**, *24*, 6954.
- [75] C. Humbert, B. Busson, A. Tadjeddine, *J. Phys. Chem. C* **2016**, *120*, 16211–16220.
- [76] A. Adamsom, A. Gast, in *Physical Chemistry of Surfaces*, 6th Ed, Wiley, New York, **1997**.
- [77] L. Cui, Z. Liu, S. Duan, D.-Y. Wu, B. Ren, Z.-Q. Tian, S.-Z. Zou, *J. Phys. Chem. B* **2005**, *109*, 17597–17602.
- [78] N. Martín Sabanés, T. Ohto, D. Andrienko, Y. Nagata, K. F. Domke, *Angew. Chem.* **2017**, *129*, 9928–9933; *Angew. Chem. Int. Ed.* **2017**, *56*, 9796–9801.
- [79] a) P. Verma, *Chem. Rev.* **2017**, *117*, 6447–6466; b) A. J. Cowan, L. J. Hardwick, *Annu. Rev. Anal. Chem.* **2019**, *12*, 323–346.
- [80] T. Touzalin, S. Joiret, E. Maisonhaute, I. T. Lucas, *Curr. Opin. Electrochem.* **2017**, *6*, 46–52.
- [81] I. Yagi, K. Inokuma, K. i. Kimijima, H. Notsu, *J. Phys. Chem. C* **2014**, *118*, 26182–26190.
- [82] J. Lahann, S. Mitragotri, T.-N. Tran, H. Kaido, J. Sundaram, I. S. Choi, S. Hoffer, G. A. Somorjai, R. Langer, *Science* **2003**, *299*, 371–374.
- [83] S. Rivera-Rubero, S. Baldelli, *J. Phys. Chem. B* **2004**, *108*, 15133–15140.
- [84] Z. D. Schultz, A. A. Gewirth, *Anal. Chem.* **2005**, *77*, 7373–7379.
- [85] B. r. Braunschweig, P. Mukherjee, D. D. Dlott, A. Wieckowski, *J. Am. Chem. Soc.* **2010**, *132*, 14036–14038.
- [86] W. Zhou, S. Inoue, T. Iwahashi, K. Kanai, K. Seki, T. Miyamae, D. Kim, Y. Katayama, Y. Ouchi, *Electrochem. Commun.* **2010**, *12*, 672–675.
- [87] N. García Rey, D. D. Dlott, *J. Phys. Chem. C* **2015**, *119*, 20892–20899.
- [88] B. A. Rosen, A. Salehi-Khojin, M. R. Thorson, W. Zhu, D. T. Whipple, P. J. Kenis, R. I. Masel, *Science* **2011**, *334*, 643–644.
- [89] a) D. Verreault, W. Hua, H. C. Allen, *J. Phys. Chem. Lett.* **2012**, *3*, 3012–3028; b) S. Nihonyanagi, S. Yamaguchi, T. Tahara, *J. Chem. Phys.* **2009**, *130*, 204704.
- [90] S. Nihonyanagi, S. Yamaguchi, T. Tahara, *Chem. Rev.* **2017**, *117*, 10665–10693.
- [91] C. L. Anfuso, D. Xiao, A. M. Ricks, C. F. Negre, V. S. Batista, T. Lian, *J. Phys. Chem. C* **2012**, *116*, 24107–24114.
- [92] M. L. Clark, B. Rudsteyn, A. Ge, S. A. Chabolla, C. W. Machan, B. T. Psciuk, J. Song, G. Canzi, T. Lian, V. S. Batista, *J. Phys. Chem. C* **2016**, *120*, 1657–1665.
- [93] M. L. Clark, A. Ge, P. E. Videla, B. Rudsteyn, C. J. Miller, J. Song, V. S. Batista, T. Lian, C. P. Kubiak, *J. Am. Chem. Soc.* **2018**, *140*, 17643–17655.
- [94] a) A. P. Willard, S. K. Reed, P. A. Madden, D. Chandler, *Faraday Discuss.* **2009**, *141*, 423–441; b) D. T. Limmer, A. P. Willard, P. Madden, D. Chandler, *Proc. Nat. Acad. Sci.* **2013**, *110*, 4200–4205; c) T. Gowthami, G. Tamilselvi, G. Jacob, G. Raina, *Phys. Chem. Chem. Phys.* **2015**, *17*, 13964–13972.
- [95] J. Carrasco, A. Hodgson, A. Michaelides, *Nat. Mater.* **2012**, *11*, 667–674.
- [96] A. M. Gardner, K. H. Saeed, A. J. Cowan, *Phys. Chem. Chem. Phys.* **2019**, *21*, 12067–12086.
- [97] A. Peremans, A. Tadjeddine, *J. Chem. Phys.* **1995**, *103*, 7197–7203.
- [98] S. Nihonyanagi, S. Ye, K. Uosaki, L. Dreesen, C. Humbert, P. Thiry, A. Peremans, *Surf. Sci.* **2004**, *573*, 11–16.
- [99] Q. Du, E. Freysz, Y. R. Shen, *Phys. Rev. Lett.* **1994**, *72*, 238.
- [100] a) K. A. Becraft, F. G. Moore, G. L. Richmond, *Phys. Chem. Chem. Phys.* **2004**, *6*, 1880–1889; b) M. Yeganeh, S. Dougal, H. Pink, *Phys. Rev. Lett.* **1999**, *83*, 1179.
- [101] Z. D. Schultz, S. K. Shaw, A. A. Gewirth, *J. Am. Chem. Soc.* **2005**, *127*, 15916–15922.
- [102] H. Noguchi, T. Okada, K. Uosaki, *Electrochim. Acta* **2008**, *53*, 6841–6844.
- [103] M. Morgenshtern, T. Michely, G. Comsa, *Phys. Rev. Lett.* **1996**, *77*, 703.
- [104] N. Ikemiyai, A. A. Gewirth, *J. Am. Chem. Soc.* **1997**, *119*, 9919–9920.
- [105] H. Noguchi, T. Okada, K. Uosaki, *Faraday Discuss.* **2009**, *140*, 125–137.
- [106] Y. Tong, F. Lapointe, M. Thämer, M. Wolf, R. K. Campen, *Angew. Chem. Int. Ed.* **2017**, *56*, 4211–4214; *Angew. Chem.* **2017**, *129*, 4275–4278.
- [107] L. B. Dreier, Z. Liu, A. Narita, M.-J. van Zadel, K. Müllen, K.-J. Tielrooij, E. H. Backus, M. Bonn, *J. Phys. Chem. C* **2019**, *123*, 24031–24038.
- [108] M. Schmidt, P. Guyot-Sionnest, *J. Chem. Phys.* **1996**, *104*, 2438–2445.
- [109] B. Persson, M. Persson, *Solid State Commun.* **1980**, *36*, 175–179.
- [110] T. C. Anglin, D. B. O'Brien, A. M. Massari, *J. Phys. Chem. C* **2010**, *114*, 17629–17637.
- [111] S. Yang, H. Noguchi, K. Uosaki, *J. Phys. Chem. C* **2015**, *119*, 26056–26063.
- [112] S. A. Sorenson, J. G. Patrow, J. M. Dawlaty, *J. Am. Chem. Soc.* **2017**, *139*, 2369–2378.
- [113] J. G. Patrow, S. A. Sorenson, J. M. Dawlaty, *J. Phys. Chem. C* **2017**, *121*, 11585–11592.
- [114] S. M. Piontek, M. DelloStretto, B. Mandal, T. Marshall, M. L. Klein, E. Borguet, *J. Am. Chem. Soc.* **2020**, *142*, 12096–12105.
- [115] A. Ge, G. Kastlunger, J. Meng, P. Lindgren, J. Song, Q. Liu, A. Zaslavsky, T. Lian, A. A. Peterson, *J. Am. Chem. Soc.* **2020**, *142*, 11829–11834.
- [116] B. Persson, A. Tadjeddine, *Phys. Rev. Lett.* **1994**, *73*, 3010.
- [117] M. I. Muglali, A. Erbe, Y. Chen, C. Barth, P. Koelsch, M. Rohwerder, *Electrochim. Acta* **2013**, *90*, 17–26.
- [118] J. D. C. Jacob, T. R. Lee, S. Baldelli, *J. Phys. Chem. C* **2014**, *118*, 29126–29134.
- [119] J. D. C. Jacob, S. Rittikulsittichai, T. R. Lee, S. Baldelli, *J. Phys. Chem. C* **2013**, *117*, 9355–9365.
- [120] R. B. Kutz, B. Braunschweig, P. Mukherjee, R. L. Behrens, D. D. Dlott, A. Wieckowski, *J. Catal.* **2011**, *278*, 181–188.
- [121] C. Lamy, *Electrochim. Acta* **1984**, *29*, 1581–1588.
- [122] D. S. Corrigan, E. K. Krauskopf, L. M. Rice, A. Wieckowski, M. J. Weaver, *J. Phys. Chem.* **1988**, *92*, 1596–1601.
- [123] R. B. Kutz, B. r. Braunschweig, P. Mukherjee, D. D. Dlott, A. Wieckowski, *J. Phys. Chem. Lett.* **2011**, *2*, 2236–2240.
- [124] Y. Liu, W. Yu, D. Raciti, D. H. Gracias, C. Wang, *J. Phys. Chem. C* **2018**, *123*, 426–432.
- [125] J. F. Gomes, B. Busson, A. Tadjeddine, *J. Phys. Chem. B* **2006**, *110*, 5508–5514.
- [126] a) A. M. El-Zohry, *Phys. Chem.* **2022**, *2*, 1–15; b) G. Neri, J. J. Walsh, G. Teobaldi, P. M. Donaldson, A. J. Cowan, *Nat. Catal.* **2018**, *1*, 952–959.
- [127] a) A. Falase, K. Garcia, C. Lau, P. Atanassov, *Electrochem. Commun.* **2011**, *13*, 1488–1491; b) A. Fielicke, P. Gruene, G. Meijer, D. M. Rayner, *Surf. Sci.* **2009**, *603*, 1427–1433.
- [128] Y. Tong, K. Cai, M. Wolf, R. K. Campen, *Catal. Today* **2016**, *260*, 66–71.
- [129] N. Zhang, Y. Zou, L. Tao, W. Chen, L. Zhou, Z. Liu, B. Zhou, G. Huang, H. Lin, S. Wang, *Angew. Chem. Int. Ed.* **2019**, *131*, 16042–16050.
- [130] a) A. Bagger, W. Ju, A. S. Varela, P. Strasser, J. Rossmeisl, *ChemPhysChem* **2017**, *18*, 3266–3273; b) Y. Hori, H. Wakebe, T. Tsukamoto, O. Koga, *Electrochim. Acta* **1994**, *39*, 1833–1839.
- [131] G. Neri, P. M. Donaldson, A. J. Cowan, *J. Am. Chem. Soc.* **2017**, *139*, 13791–13797.
- [132] Z.-C. Huang-Fu, Q.-T. Song, Y.-H. He, J.-J. Wang, J.-Y. Ye, Z.-Y. Zhou, S.-G. Sun, Z.-H. Wang, *Phys. Chem. Chem. Phys.* **2019**, *21*, 25047–25053.
- [133] S.-G. Sun, W.-B. Cai, L.-J. Wan, M. Osawa, *J. Phys. Chem. B* **1999**, *103*, 2460–2466.
- [134] C. L. Anfuso, A. M. Ricks, W. Rodríguez-Córdoba, T. Lian, *J. Phys. Chem. C* **2012**, *116*, 26377–26384.
- [135] Z. Wang, J. A. Carter, A. Lagutchev, Y. K. Koh, N.-H. Seong, D. G. Cahill, D. D. Dlott, *Science* **2007**, *317*, 787–790.
- [136] A. Ge, B. Rudsteyn, P. E. Videla, C. J. Miller, C. P. Kubiak, V. S. Batista, T. Lian, *Acc. Chem. Res.* **2019**, *52*, 1289–1300.
- [137] Z. J. Zhang, P. Ramadass, *Batteries for Sustainability*, Springer, **2013**, pp. 319–357.
- [138] P. Verma, P. Maire, P. Novák, *Electrochim. Acta* **2010**, *55*, 6332–6341.

- [139] H. Liu, Y. Tong, N. Kuwata, M. Osawa, J. Kawamura, S. Ye, *J. Phys. Chem. C* **2009**, *113*, 20531–20534.
- [140] L. Yu, H. Liu, Y. Wang, N. Kuwata, M. Osawa, J. Kawamura, S. Ye, *Angew. Chem., Int. Ed.* **2013**, *52*, 5753–5756.
- [141] S. K. Heiskanen, J. Kim, B. L. Lucht, *Joule* **2019**, *3*, 2322–2333.
- [142] P. Mukherjee, A. Lagutchev, D. D. Dlott, *J. Electrochem. Soc.* **2011**, *159*, A244.
- [143] B. G. Nicolau, N. García-Rey, B. Dryzhakov, D. D. Dlott, *J. Phys. Chem. C* **2015**, *119*, 10227–10233.
- [144] Y. Horowitz, H.-L. Han, P. N. Ross, G. A. Somorjai, *J. Am. Chem. Soc.* **2016**, *138*, 726–729.
- [145] Y. Horowitz, H.-L. Han, G. A. Somorjai, *Ind. Eng. Chem. Res.* **2018**, *57*, 1480–1486.
- [146] N.-S. Choi, K. H. Yew, K. Y. Lee, M. Sung, H. Kim, S.-S. Kim, *J. Power Sources* **2006**, *161*, 1254–1259.
- [147] M. McArthur, S. Trussler, J. Dahn, *J. Electrochem. Soc.* **2011**, *159*, A198.
- [148] Y. Horowitz, H.-G. Steinruck, H.-L. Han, C. Cao, I. I. Abate, Y. Tsao, M. F. Toney, G. A. Somorjai, *Nano Lett.* **2018**, *18*, 2105–2111.
- [149] Y. Horowitz, H.-L. Han, F. A. Soto, W. T. Ralston, P. B. Balbuena, G. A. Somorjai, *Nano Lett.* **2018**, *18*, 1145–1151.
- [150] J. Z. Olson, P. K. Johansson, D. G. Castner, C. W. Schlenker, *Chem. Mater.* **2018**, *30*, 1239–1248.

Manuscript received: February 8, 2022

Accepted manuscript online: June 22, 2022

Version of record online: July 21, 2022